Investigation of Sea Spray Effect on the Vertical Momentum Transport Using an Eulerian Multifluid-Type Model

YEVGENII RASTIGEJEV[a,b] AND SERGEY A. SUSLOV[c]

[a] *Department of Mathematics and Statistics, North Carolina Agricultural and Technical State University, Greensboro, North Carolina*
[b] *Applied Science and Technology Ph.D. Program, North Carolina Agricultural and Technical State University, Greensboro, North Carolina*
[c] *Swinburne University of Technology, Hawthorn, Victoria, Australia*

(Manuscript received 12 June 2021, in final form 18 October 2021)

ABSTRACT: The Eulerian multifluid mathematical model is developed to describe the marine atmospheric boundary layer laden with sea spray under the high-wind condition of a hurricane. The model considers spray and air as separate continuous interacting turbulent media and employs the multifluid E–ϵ closure. Each phase is described by its own set of coupled conservation equations and characterized by its own velocity. Such an approach enables us to accurately quantify the interaction between spray and air and pinpoint the effect of spray on the vertical momentum transport much more precisely than could be done with traditional mixture-type approaches. The model consistently quantifies the effect of spray inertia and the suppression of air turbulence due to two different mechanisms: the turbulence attenuation, which results from the inability of spray droplets to fully follow turbulent fluctuations, and the vertical transport of spray against the gravity by turbulent eddies. The results of numerical and asymptotic analyses show that the turbulence suppression by spray overpowers its inertia several meters above wave crests, resulting in a noticeable wind acceleration and the corresponding reduction of the drag coefficient from the reference values for a spray-free atmosphere. This occurs at much lower than predicted previously spray volume fraction values of $\sim 10^{-5}$. The falloff of the drag coefficient from its reference values is more strongly pronounced at higher altitudes. The drag coefficient reaches its maximum at spray volume fraction values of $\sim 10^{-4}$, which is several times smaller than predicted by mixture-type models.

KEYWORDS: Fluxes; Turbulence; Tropical cyclones; Air-sea interaction; Hurricanes/typhoons; Numerical analysis/modeling; Marine boundary layer

1. Introduction

Over the past several decades, substantial evidence based on measurements and theoretical analysis has emerged that sea spray strongly affects the dynamics and structure of tropical cyclones (TCs) by modifying the vertical heat (the thermodynamic effect of spray) and momentum (the mechanical effect of spray) fluxes throughout a marine atmospheric boundary layer (MABL). The spray presence also influences the balance between heat influx and momentum outflux through the ocean surface, which are the wind accelerating and decelerating factors, respectively. Despite the effort made over the past years to quantify various spray influences (e.g., Ling and Kao 1976; Mestayer and Lefauconnier 1988; Fairall et al. 1994; Lighthill 1999; Makin 2004; Barenblatt et al. 2005; Bianco et al. 2011; Rastigejev et al. 2011; Toffoli et al. 2011; Rastigejev and Suslov 2014, hereinafter RS14; Veron 2015; Wu et al. 2015; Rastigejev and Suslov 2016; Tang et al. 2017; He et al. 2018; Rastigejev and Suslov 2019; Ma et al. 2020; Peng and Richter 2020; Vanderplow et al. 2020), their full understanding is still lacking largely due to significant difficulties with mathematical and computational modeling of large-scale turbulent multiphase flows.

In this work we present a study of the spray effect on the air–sea momentum exchange. Momentum transfer in turbulent flows seeded with particles have been studied via direct numerical simulation (e.g., Dritselis and Vlachos 2008, 2011; Richter and Sullivan 2013, 2014). Unfortunately, such studies require very heavy computational resources and currently have to be limited to flows characterized by the values of Reynolds number that are many orders of magnitude smaller than those corresponding to realistic MABL flows occurring at hurricane speeds and on the oceanic wavelength scale. Traditionally, such studies employ Eulerian mixture-type models (Andreas 2004; Makin 2004; Barenblatt et al. 2005; Kudryavtsev 2006; Rastigejev et al. 2011; RS14). A common assumption that mixture-type models use is that the horizontal velocity components of air and spray droplets are equal while the vertical ones differ by the value of the droplet terminal velocity in quiescent air. This results in the governing equations for mixture-type model being similar in form to the ones used for a single-phase flow. In particular, a single momentum equation is solved for both air and spray. The mixture-type models for the MABL flow configuration are frequently simplified further compared with those for a general turbulent multiphase flow. Specifically, the vertical momentum equation may be omitted (Rastigejev et al. 2011; RS14) since it becomes identical to the spray continuity equation and, hence, redundant. While the mixture-type approach is much simpler than the multifluid one, generally it does not allow a consistent description of the interaction between air and spray in a turbulent flow and may lead to inaccurate results.

Corresponding author: Yevgenii Rastigejev, ye_rast@yahoo.com

DOI: 10.1175/JPO-D-21-0127.1

To address these shortcomings, we have developed an Eulerian multifluid model of a spray-laden MABL. In this approach, spray and air are considered separately. Each phase is described by its own set of coupled equations for mass, momentum, and turbulent kinetic energy (TKE) and is characterized by its own velocity. Such an approach enables us to accurately quantify the interaction between spray and air and pinpoint the effect of spray on the vertical momentum transport in MABL much more precisely compared with a more traditional mixture-type approach. In this paper we compare the results of the newly developed multiphase model with the previous mixture model (RS14). This comparison enables us to judge the importance of additional physical factors captured by the multiphase model.

In particular, the multifluid approach enables us to quantify consistently the suppression of turbulence intensity in the air due to two different mechanisms: the turbulence attenuation (TA), which results from the inability of spray droplets to fully follow turbulent fluctuations (Hetsroni and Sokolov 1971; Danon et al. 1977; Levy and Lockwood 1981), and the vertical transport of spray against gravity by the turbulent flow (Barenblatt 1953; Barenblatt et al. 2005), also known as gravity lubrication (GL). Both GL and TA effects lead to the increase of the airflow velocity due to the reduction of the vertical turbulent transport. Hence, they are referred to as the "accelerating" effects. Even though the GL effect was accounted for within the RS14 mixture model, its quantitative description could be insufficiently accurate since spray vertical profiles, which define the magnitude of GL, produced by mixture-type and the multifluid models differ noticeably. The magnitude of the turbulent energy dissipation caused by TA due to the interaction between air and spray droplets depends sensitively on the details of their relative motion. Therefore, the spray-caused TA and the related suppression of air turbulence can be quantified consistently only within the multifluid framework that accurately models such a relative motion. The multifluid model accounts for two decelerating effects of spray inertia. The first one is caused by the relatively high spray concentration near the ocean surface that increases the mass density of the air–spray mixture, which leads to the local wind speed reduction compared to the reference logarithmic profile. The second decelerating effect is due to the transfer of the air momentum to accelerating sea spray torn from the wave crests. The former effect can be sufficiently accurately described by mixture-type models, as indeed has been done in RS14. However, such models are incapable of capturing the latter effect since this requires taking into account the local velocity difference between the injected spray and the surrounding air–spray mixture.

Our multifluid model also revealed that the local terminal speed of spray droplets decreases in a turbulent flow compared with that in the quiescent air due to a larger air–droplet drag. This decrease in the local terminal speed causes a higher spray concentration below the wave-crest level since a slower downward motion of spray droplets leads to their accumulation in this region. Our calculations show that for the same intensity of spray sources the spray concentrations at the wave-crest level predicted by the multifluid model can be twice as high as that predicted by mixture-type models that assume that the droplet terminal speed remains equal to that in quiescent air. Taking into account such an increase of spray concentration is important since the magnitude of both thermodynamic and mechanical spray effects depends strongly on it.

The numerical and analytic results obtained for a spray-laden MABL using the multifluid model show that the spray lubrication and inertia balance each other in the vicinity of the wave-crest level, where the spray source is located and the concentration of spray is high. However, several meters above wave crests the lubrication effect starts dominating over spray inertia. As a consequence, wind becomes stronger and the drag coefficient decreases compared with its reference value for a spray-free atmosphere. A noticeable reduction of the drag coefficient occurs for spray volume fraction as low as $\sim 10^{-5}$. The drag coefficient continues to fall off its reference value as the wind speed increases, reaching its maximum at spray volume fraction $\sim 10^{-4}$. The range of spray concentration values, $\sim 10^{-5}$–$\sim 10^{-4}$, for which the above effects are detected is significantly lower than that predicted by mixture-type models (Rastigejev et al. 2011; RS14). The actual flow speed at which the drag coefficient reaches its maximum depends on the adopted correlation law between the wind speed and the spray production intensity. The developed model also confirms that the degree of the wind speed increase and the behavior of the drag coefficient vary with altitude. Therefore, the spray influence on the turbulent flow cannot be conclusively characterized by the value of the drag coefficient at any one level. Rather, it should be considered as a sensitive function of the elevation above the sea level.

While the current multifluid model formulated in sections 2–4, with technical derivation details given in the appendix, is capable of describing the air–spray interaction more accurately than the mixture model developed in RS14 with just a moderate increase of a computational cost, it does not make RS14 obsolete. Rather, it states its findings, complements them with new features, and puts them on a solid physical foundation. In turn, a simpler RS14 model, which, as we show in section 5, corresponds to the limiting fine-spray case of the current model, provides a qualitative validity check for the current model. In section 7 the asymptotic analysis of the current model is carried out for droplets with radii $\lesssim 200\,\mu$m at hurricane wind speeds and for small spray concentrations. It enables us to obtain approximate analytic expressions for the vertical spray distribution and spray velocity profile that are used to define the interface condition for spray concentration at the wave-crest level required for a numerical implementation of the model. Predictions made using the current model and the newly detected effects not captured by RS14 that follow from the model analysis reported in section 6 are discussed in section 8. The summarizing discussion of the new results and their comparison with those of RS14 are given in section 9.

2. Governing equations

a. Mass and momentum conservation

We consider a horizontally homogeneous spray-laden turbulent flow in MABL at high wind speeds with the spume

spray generated at the average wave-crest level z_w. For mathematical description of such a flow we employ an Eulerian two-fluid-type model that considers both gas (air) and liquid (water droplet) phases as separate interpenetrating continuous media. Three-dimensional continuity and momentum equations for this model are given in section a of the appendix. For simplicity of notation we omit the overbars and hats for ensemble-average and mass-weighted average values introduced there and denote them by tildes in the text below.

It is shown in the appendix that the continuity equations for air and spray reduce to the following algebraic relationships

$$\tilde{w}_a = 0, \quad \tilde{s}\tilde{w}_w = -a_0 s_0 \tilde{H}_{\tilde{z}-z_w}, \tag{1}$$

where $\tilde{z}$ is the vertical coordinate; a_0 is the droplet terminal speed in quiescent air; s_0 is characteristic value of the spray volume fraction; $\tilde{w}_a$ and $\tilde{w}_w$ are the mass-weighted average vertical velocities of air and spray, respectively; and $\tilde{s}$ is the ensemble average spray volume fraction. The spray production distribution source function $\tilde{H}_{\tilde{z}}$ is defined in section a of the appendix.

The momentum conservation equations for the vertical and horizontal directions are written separately for air and spray as

$$\frac{d}{d\tilde{z}}\left(\tilde{k}_a \frac{d\tilde{u}_a}{d\tilde{z}}\right) + \frac{\sigma}{\tilde{\tau}_d}\tilde{s}(\tilde{u}_w - \tilde{u}_a) = 0, \tag{2}$$

$$\frac{d}{d\tilde{z}}\left(\tilde{k}_w \tilde{s} \frac{d\tilde{u}_w}{d\tilde{z}}\right) - \tilde{s}\tilde{w}_w \frac{d\tilde{u}_w}{d\tilde{z}} + \frac{\tilde{s}}{\tilde{\tau}_d}(\tilde{u}_a - \tilde{u}_w) + (U - \tilde{u}_w)a_0 s_0 \tilde{\delta}_{\tilde{z}-z_w} = 0, \tag{3}$$

$$\frac{d}{d\tilde{z}}\left(\frac{4}{3}\tilde{k}_w \tilde{s} \frac{d\tilde{w}_w}{d\tilde{z}} - \frac{2}{3}\tilde{s}\tilde{e}_w\right) - \tilde{s}\tilde{w}_w \frac{d\tilde{w}_w}{d\tilde{z}} - \tilde{s}g + \frac{\tilde{s}}{\tilde{\tau}_d}(\tilde{w}_d - \tilde{w}_w) + (W - \tilde{w}_w)a_0 s_0 \tilde{\delta}_{\tilde{z}-z_w} = 0, \tag{4}$$

where Eqs. (2)–(4) describe the variation of the average horizontal air ($\tilde{u}_a$) and spray ($\tilde{u}_w$) and vertical spray ($\tilde{w}_w$) velocities, respectively. Here $\tilde{k}_a$ and $\tilde{k}_w$ are turbulent eddy viscosities of air and water phases, respectively; U and W are the horizontal and vertical injection velocity components of spray droplets entering the air at the wave-crest level, respectively; $\tilde{\tau}_d$ is the droplet relaxation time over which droplets adjust their velocity to the local condition of force equilibrium; g is the gravity acceleration; and $\sigma = \rho_w/\tilde{\rho}_a$ is the ratio of water and average air densities.

b. Turbulence model

We employ a multiphase E–ϵ (aka k–ϵ) model for the turbulent kinetic energy of air ($\tilde{e}_a$) and its dissipation rate ($\tilde{\epsilon}_a$):

$$\alpha_e \frac{d}{d\tilde{z}}\left(\tilde{\rho}_a \tilde{k}_a \frac{d\tilde{e}_a}{d\tilde{z}}\right) = \tilde{\rho}_a(\tilde{\epsilon}_a - \tilde{p}_a) - \tilde{q}_{ae}, \tag{5}$$

$$\alpha_\epsilon \frac{d}{d\tilde{z}}\left(\tilde{\rho}_a \tilde{k}_a \frac{d\tilde{\epsilon}_a}{d\tilde{z}}\right) = \tilde{\rho}_a\left(\tilde{d}_{a\epsilon} - \tilde{p}_{a\epsilon}\right) - \tilde{q}_{a\epsilon}, \tag{6}$$

where

$$\tilde{q}_{ae} = \frac{\tilde{s}\rho_w}{\tilde{\tau}_d}\left(\tilde{q}_{aw} - 2\tilde{e}_a + \tilde{\mathbf{u}}^r \cdot \tilde{\mathbf{u}}^d\right), \quad \tilde{k}_a = \frac{(\alpha\tilde{e}_a)^2}{\tilde{\epsilon}_a},$$

$$\tilde{p}_a = \frac{d\tilde{u}_a}{d\tilde{z}}\left(\tilde{k}_a \frac{d\tilde{u}_a}{d\tilde{z}}\right) + \tilde{d}_{aw} g \frac{\rho_w}{\tilde{\rho}} \frac{d\tilde{s}}{d\tilde{z}}, \quad \tilde{\rho} = \tilde{\rho}_a + \rho_w \tilde{s},$$

$$\tilde{p}_{a\epsilon} = C_{\epsilon,1}\frac{\tilde{\epsilon}_a \tilde{p}_a}{\tilde{e}_a}, \quad \tilde{d}_\epsilon = C_{\epsilon,2}\frac{\tilde{\epsilon}_a^2}{\tilde{e}_a}, \quad \tilde{q}_{a\epsilon} = C_{\epsilon,3}\frac{\tilde{\epsilon}_a \tilde{q}_{ae}}{\tilde{e}_a}.$$

The air and droplet turbulent energies and the air–droplet fluctuating velocity covariance are given by

$$\tilde{e}_a = \frac{1}{2}\widehat{\tilde{u}'_{ak}\tilde{u}'_{ak}}, \quad \tilde{e}_w = \frac{1}{2}\widehat{\tilde{u}''_{wk}\tilde{u}''_{wk}}, \quad \tilde{q}_{aw} = \widehat{\tilde{u}''_{wk}\tilde{u}'_{ak}},$$

respectively. Note that, unlike equations of the E–ϵ model considered in our previous works (RS14; Rastigejev and Suslov 2016, 2019), equations of the modified model (5) and (6) contain additional terms $\tilde{q}_{ae}$ and $\tilde{q}_{a\epsilon}$ (Elghobashi and Abou-Arab 1983) that represent the influence of droplets on the air turbulence due to the air–droplet interaction (Gore and Crowe 1989).

c. Turbulence closures

The expressions for the drift velocity $\tilde{\mathbf{u}}^d$, which accounts for the dispersion of droplets by the turbulent air motion, and the turbulent diffusion velocity of spray $\tilde{\mathbf{u}}^f$, which is the difference between the mass and ensemble average velocities of spray, read (Simonin and Viollet 1990)

$$\tilde{\mathbf{u}}^d = \frac{\overline{s'\mathbf{u}'_a}}{\tilde{s}} = -\tilde{d}_{aw}\frac{\nabla\tilde{s}}{\tilde{s}}, \quad \tilde{\mathbf{u}}^f = \frac{\overline{s'\mathbf{u}'_w}}{\tilde{s}} = -\tilde{d}_w\frac{\nabla\tilde{s}}{\tilde{s}}. \tag{7}$$

The turbulent diffusion coefficients are derived in Simonin (1991) as

$$\tilde{d}_{aw} = \frac{1}{3}\tilde{q}_{aw}\tilde{\tau}^t_{aw}, \quad \tilde{d}_w = \frac{2}{3}\tilde{e}_a\tilde{\tau}^t_{aw}, \quad \tilde{k}_a = \frac{2}{3}\tilde{e}_a\tilde{\tau}^t_a,$$

$$\tilde{k}_w = \frac{1}{3}(\tilde{\tau}^t_{aw}\sigma'_0\tilde{q}_{aw} + \tilde{\tau}_d\tilde{e}_w). \tag{8}$$

The turbulent energies, the characteristic times of turbulent exchange, the droplet relaxation times, and the droplet Reynolds number are given by

$$\tilde{q}_{aw} = 2c_1\tilde{e}_a, \quad \tilde{e}_w = c_1\tilde{e}_a, \quad \tilde{\tau}^t_{aw} = c_0\tilde{\tau}^t_a,$$

$$\tilde{\tau}^t_a = \frac{3\alpha^2}{2}\frac{\tilde{e}_a}{\tilde{\epsilon}_a}, \quad \tilde{\tau}_{d,st} = \frac{2r^2\sigma}{9\nu},$$

$$\tilde{\tau}_d = \tilde{\tau}_{d,st}\left(1 + 0.15\,\mathrm{Re}_d^{0.687}\right)^{-1}, \quad \mathrm{Re}_d = \frac{2r\langle|\tilde{\mathbf{u}}^r|\rangle}{\nu}, \tag{9}$$

where

$$c_0 = \frac{1}{\sigma'_0\sqrt{1 + C_\beta\xi_r^2}}, \quad c_1 = \frac{\tilde{\tau}^t_{aw}}{\tilde{\tau}_d + \tilde{\tau}^t_{aw}}, \quad \xi_r = \frac{\langle|\tilde{\mathbf{u}}^r|\rangle}{\sqrt{\frac{2}{3}\tilde{e}_a}},$$

$$C_\beta = 0.45 + 1.35\sin^2\theta, \ \sin\theta = \frac{|\tilde{\mathbf{u}}_w|^2 - \tilde{\mathbf{u}}_a \cdot \tilde{\mathbf{u}}_w}{|\tilde{\mathbf{u}}_w - \tilde{\mathbf{u}}_a||\tilde{\mathbf{u}}_w|}. \tag{10}$$

Here a simple analytical expression developed in Tchen's theory of discrete particle dispersion (Hinze 1975) is employed

to define turbulent energy $\tilde{e}_w$ of spray droplets and the air–droplet fluctuating velocity covariance $\tilde{q}_{aw}$ via turbulent energy of air $\tilde{e}_a$. Factor $c_1 < 1$, which is the ratio of the eddy time to the sum of that and the droplet relaxation time, quantifies the capacity of the carrier phase (air) to transfer turbulent kinetic energy to the carried dispersed phase (droplets).

The turbulent eddy–droplet interaction time $\tilde{\tau}^t_{aw}$ is obtained by multiplying turbulent eddy time $\tilde{\tau}^t_a$ by c_0, which accounts for the so-called crossing-trajectories effect (Yudine 1959; Csanady 1963) when droplets do not remain trapped by the successive eddies but rather pass through them due to their inertia. The coefficient C_β in expression for c_0 depends on the angle θ between vectors $\tilde{\mathbf{u}}_w - \tilde{\mathbf{u}}_a$ and $\tilde{\mathbf{u}}_w$.

The particle relaxation time $\tilde{\tau}_d$ is given by a commonly used semiempirical analytical expression (Clift et al. 1978). The root-mean-square (RMS) of the local relative air–droplet velocity $\langle|\tilde{\mathbf{u}}^r|\rangle$ is defined as follows:

$$\langle|\tilde{\mathbf{u}}^r|\rangle = \sqrt{\tilde{\mathbf{u}}^r \cdot \tilde{\mathbf{u}}^r + 2(\tilde{e}_a + \tilde{e}_w - \tilde{q}_{aw})} = \sqrt{\tilde{\mathbf{u}}^r \cdot \tilde{\mathbf{u}}^r + 2\tilde{e}_a(1 - c_1)}, \tag{11}$$

where $\tilde{\mathbf{u}}^r$ is the mass average relative velocity between water and air phases defined by (A5). The values of parameters entering the modified E–ϵ turbulence model are (Simonin and Viollet 1990)

$$\alpha = 0.3, \quad \alpha_e = 1, \quad \alpha_\epsilon = 0.77, \quad \sigma^t_0 = 0.67,$$
$$C_{\epsilon,1} = 1.44, \quad C_{\epsilon,2} = 1.92, \quad C_{\epsilon,3} = 1.$$

After substituting the expression for mass-weighted average velocity $\tilde{w}_w$ (1) and the z component of the diffusion velocity (7) into (A7) we obtain the expression for the ensemble average vertical velocity of spray droplets

$$\tilde{\mathbf{w}}_w = \frac{\tilde{d}_w}{\tilde{s}}\frac{d\tilde{s}}{d\tilde{z}} - \frac{a_0 s_0}{\tilde{s}}\tilde{H}_{\tilde{z}-z_w}. \tag{12}$$

d. Boundary conditions

To close the problem formulation we have to specify boundary conditions both at the upper and lower edges of MABL. However, the region below the wave-crest level, $z < z_w$, is periodically flooded with ocean water and modeling it, even qualitatively, is beyond the reach and scope of the current study. Instead, we consider this region rather formally using minimalistic approach with the sole goal of coming up with a plausible interface condition at $z = z_w$ so that the solution above the wave-crest level, which is of interest here, can be obtained. Having said this, we formally require that at some level $\tilde{z} = z_{0c}$, $\tilde{z}_0 < \tilde{z}_{0c} < z_w$, where $\tilde{z}_0 = 0.015u^2_\star/g$, the model solution satisfies

$$\tilde{u}_a = \frac{u_\star}{k_p}\ln\frac{\tilde{z}_{0c}}{\tilde{z}_0} = \tilde{u}_w, \quad \tilde{e}_a = \frac{u^2_\star}{\alpha}, \quad \tilde{\epsilon}_a = \frac{u^3_\star}{k_p\tilde{z}_{0c}}. \tag{13}$$

Since we do not aspire to model the sub-wave-crest region, in computations the value of $\tilde{z}_{0c}$ is chosen to avoid a very steep velocity gradient existing at the bottom edge of the logarithmic velocity profile. The condition $\tilde{u}_w = \tilde{u}_a$ is obtained from the asymptotic analysis of (3) that will be given in section 7. The last two conditions reflect the assumption that the turbulent kinetic energy and its dissipation rate under the wave-crest level obey standard distributions corresponding to the E–ϵ turbulence model.

The boundary conditions at the upper edge of MABL $\tilde{z} = \tilde{z}_\infty$ are

$$\tilde{k}_a\frac{d\tilde{u}_a}{d\tilde{z}} = u^2_\star, \quad \tilde{u}_w = \tilde{u}_a, \quad \tilde{w}_w = 0,$$
$$\frac{d\tilde{e}_a}{d\tilde{z}} = 0, \quad \frac{d\tilde{\epsilon}_a}{d\tilde{z}} = -\frac{\tilde{\epsilon}_a}{\tilde{z}_\infty}. \tag{14}$$

They represent the assumptions that the airflow above MABL is uniformly turbulent with the vertical momentum flux parameterized by the square of the friction velocity $u^2_\star$ and that the distribution of the turbulent kinetic energy and its dissipation rate are given by the E–ϵ model.

3. Nondimensional equations

The nondimensionalization is done using the following scalings:

$$\tilde{z} = z_w z, \quad \tilde{s} = s_0 s, \quad \tilde{p}_a = \frac{u^3_\star}{z_w}\,p_a,$$
$$(\tilde{u}_a, \tilde{u}_w, U, W, \tilde{\mathbf{u}}^r, \langle|\tilde{\mathbf{u}}^r|\rangle, \tilde{w}^d_w) = u_\star(u_a, u_w, u, w, \mathbf{u}^r, \langle|\mathbf{u}^r|\rangle, w^d_w),$$
$$(\tilde{w}_a, \hat{w}_w, \tilde{\mathbf{w}}_w) = a_0(w_a, w_w, \mathbf{w}_w),$$
$$(\tilde{e}_a, \tilde{e}_w, \tilde{q}_{aw}) = u^2_\star(e_a, e_w, q_{aw}), \quad \tilde{\epsilon}_a = \frac{u^3_\star}{z_w}\,\epsilon_a,$$
$$\tilde{\tau}_d = \tau_{d0}\tau_d, \quad (\tilde{\tau}^t_a, \tilde{\tau}^t_{aw}) = \frac{z_w}{u_\star}(\tau^t_a, \tau^t_{aw}),$$
$$(\tilde{k}_a, \tilde{k}_w, \tilde{d}_w, \tilde{d}_{aw}) = u_\star z_w(k_a, k_w, d_w, d_a w), \tag{15}$$

where $\tau_{d0} = a_0/g$ and $\tilde{\mathbf{w}}_w$ is an ensemble average spray velocity defined in section a of the appendix. Note that variable τ_d can be interpreted as the nondimensional local droplet relaxation time or the absolute value of the nondimensional local droplet terminal speed. Below we refer to it both ways depending on the context.

Expressions (1) take the form

$$w_a = 0, \quad sw_w = -H_{z-1}, \tag{16}$$

After substituting expression for w_w from (16) into (3) and (4) the governing equations become

$$\frac{d}{dz}\left(k_a\frac{du_a}{dz}\right) - \pi_{18}s\frac{(u_a - u_w)}{\tau_d} = 0, \tag{17}$$

$$\frac{d}{dz}\left(k_w s\frac{du_w}{dz}\right) + \pi_1\frac{du_w}{dz}H_{z-1} + \frac{s}{\pi_{17}}\frac{(u_a - u_w)}{\tau_d} + \pi_1(u - u_w)\delta_{z-1} = 0, \tag{18}$$

$$\frac{4}{3}\frac{d}{dz}\left[k_w\left(\frac{d\ln s}{dz}H_{z-1} + \delta_{z-1}\right)\right] - \frac{2}{3\pi_1}\frac{d}{dz}(se_w) - \pi_1\frac{d}{dz}\left(\frac{H_{z-1}}{s}\right) - \frac{s}{\pi_{17}} + w\delta_{z-1} + \frac{1}{\pi_{17}\tau_d}\left(\frac{s}{\pi_1}w^d + H_{z-1}\right) = 0, \tag{19}$$

$$\alpha_e \frac{d}{dz}\left(k_a \frac{de_a}{dz}\right) = \epsilon_a - p_a - q_{ae}, \tag{20}$$

$$\alpha_\epsilon \frac{d}{dz}\left(k_a \frac{d\epsilon_a}{dz}\right) = d_{a\epsilon} - p_{a\epsilon} - q_{a\epsilon}, \tag{21}$$

where

$$\begin{aligned}
&q_{ae} = \pi_{18}\frac{s}{\tau_d}\left(q_{aw} - 2e_a + \mathbf{u}^r\cdot\mathbf{u}^d\right), \quad k_a = \frac{(\alpha e_a)^2}{\epsilon_a},\\
&p_a = \frac{du_a}{dz}\left(k_a\frac{du_a}{dz}\right) + p_{ag}, \quad p_{ag} = \pi_{12}\frac{d_{aw}}{\rho}\frac{ds}{dz},\\
&p_{a\epsilon} = C_{\epsilon,1}\frac{\epsilon_a p_a}{e_a}, \quad d_\epsilon = C_{\epsilon,2}\frac{\epsilon_a^2}{e_a}, \quad q_{a\epsilon} = C_{\epsilon,3}\frac{\epsilon_a q_{ae}}{e_a},\\
&\rho = 1 + \sigma s_0 s,
\end{aligned} \tag{22}$$

and (u, w) are the horizontal and vertical components of the nondimensional velocity with which spray droplets are injected into MABL at the wave-crest level. Our computations showed that numerical results are virtually insensitive to the choice of the u and w values up to 2–5 m s^{-1}. Thus, to reduce the dimensionality of the explored parametric space we set $u = w = 0$ when reporting numerical results in the subsequent sections. The nondimensional quantities in (7)–(12) are given by

$$\begin{aligned}
&\mathbf{u}^d = -d_{aw}\frac{\nabla s}{s}, \quad \mathbf{u}^f = -d_w\frac{\nabla s}{s},\\
&d_{aw} = \frac{1}{3}q_{aw}\tau'_{aw}, \quad d_w = \frac{2}{3}e_a\tau'_{aw},\\
&k_w = \frac{1}{3}\left(\tau'_{aw}\sigma'_0 q_{aw} + \pi_{17}\tau_d e_w\right), \quad k_a = \frac{2}{3}e_a\tau'_a,\\
&q_{aw} = 2c_1 e_a, \quad e_w = c_1 e_a,\\
&\tau'_{aw} = c_0\tau'_a, \quad \tau'_a = \frac{3\alpha^2}{2}\frac{e_a}{\epsilon_a}, \quad \tau_d = \frac{1 + 0.15\,\mathrm{Re}_{d0}^{0.687}}{1 + 0.15\,\mathrm{Re}_d^{0.687}},\\
&\mathrm{Re}_d = \mathrm{Re}_{d\star}\langle|\mathbf{u}^r|\rangle, \quad c_1 = \frac{\tau'_{aw}}{\pi_{17}\tau_d + \tau'_{aw}},\\
&\xi_r = \langle|\mathbf{u}^r|\rangle\sqrt{\frac{3}{2e_a}}, \quad \langle|\mathbf{u}^r|\rangle = \sqrt{\mathbf{u}^r\cdot\mathbf{u}^r + 2e_a(1-c_1)},\\
&\mathbf{u}^r = \left(u_w - u_a, \pi_1 w_w - w^d\right),\\
&\mathbf{w}_w = -\frac{H_{z-1}}{s} + \frac{d_w}{\pi_1}\frac{1}{s}\frac{ds}{dz},
\end{aligned} \tag{23}$$

where

$$\mathrm{Re}_{d\star} = \frac{2ru_\star}{\nu}, \quad \mathrm{Re}_{d0} = \frac{2ra_0}{\nu}.$$

The nondimensional boundary conditions are

$$u_a = \frac{1}{k_p}\ln\frac{z_{0c}}{z_0} = u_w, \quad e_a = \frac{1}{\alpha}, \quad \epsilon_a = \frac{1}{k_p z_{0c}}, \tag{24}$$

at $z = z_{0c}$ and

$$k_a\frac{du_a}{dz} = 1, \quad u_w = u_a, \quad w_w = 0, \tag{25}$$

$$\frac{de_a}{dz} = 0, \quad \frac{d\epsilon_a}{dz} = -\frac{\epsilon_a}{z_\infty}, \tag{26}$$

at $z = z_\infty$.

The independent π parameters are defined as follows

$$\begin{aligned}
&\pi_{12} = \frac{g\sigma s_0 z_w}{u_\star^2}, \quad \pi_{17} = \frac{\tau_{d0}u_\star}{z_w} = \frac{a_0 u_\star}{g z_w},\\
&\pi_{18} = \frac{z_w\sigma s_0}{\tau_{d0}u_\star} = \frac{\sigma s_0}{\pi_{17}}.
\end{aligned} \tag{27}$$

For convenience we also use

$$\pi_1 = \frac{\pi_{12}}{\pi_{18}} = \frac{a_0}{u_\star}. \tag{28}$$

Parameters π_1 and π_{12} are defined as in Rastigejev and Suslov (2016, 2019) (with α_s set to 1). Parameters first introduced in this paper have indexes starting with 17 to ensure consistency and continuity with our previous articles.

4. Further simplification of the mathematical model

Given that spray is produced in a very thin layer near the wave-crest level, it is reasonable to parameterize the spray production source assuming that δ_{z-1} and its integral $1 - H_{z-1}$ are Dirac and Heaviside functions, respectively. Then each of the spray momentum conservation equations (18) and (19) can be written as two separate equations for the regions below ($z < 1$) and above ($z > 1$) the wave-crest level, respectively, coupled via the interface boundary conditions enforcing the continuity of distributions of various physical quantities across the wave-crest level $z = 1$ but allowing the jump in its derivatives (fluxes) that occurs due the presence of a localized spray source. For $z < 1$ we then have

$$\frac{d}{dz}\left(k_w s\frac{du_w}{dz}\right) + \pi_1\frac{du_w}{dz} + \frac{s}{\pi_{17}}\frac{u_a - u_w}{\tau_d} = 0, \tag{29}$$

$$\begin{aligned}
&\frac{4}{3}\frac{d}{dz}\left(k_w\frac{d\ln s}{dz}\right) - \frac{2}{3\pi_1}\frac{d}{dz}(se_w) + \frac{\pi_1}{s^2}\frac{ds}{dz}\\
&\quad - \frac{s}{\pi_{17}} - \frac{1}{\pi_{17}\tau_d}\left(\frac{d_{aw}}{\pi_1}\frac{ds}{dz} - 1\right) = 0,
\end{aligned} \tag{30}$$

while for $z > 1$

$$\frac{d}{dz}\left(k_w s\frac{du_w}{dz}\right) + \frac{s}{\pi_{17}}\frac{u_a - u_w}{\tau_d} = 0, \tag{31}$$

$$\frac{2}{3}\pi_{17}\frac{d}{dz}(se_w) + \pi_1 s + \frac{d_{aw}}{\tau_d}\frac{ds}{dz} = 0. \tag{32}$$

The interface conditions are

$$\left.\frac{du_w}{dz}\right|_{z=1^+} - \left.\frac{du_w}{dz}\right|_{z=1^-} + \pi_1\left.\frac{u - u_w}{k_w s}\right|_{z=1} = 0, \tag{33}$$

$$-\frac{4k_w}{3}\frac{d\ln s}{dz}\bigg|_{z=1^-}+\frac{\pi_1}{s(1)}+w=0, \tag{34}$$

$$s(1)=\frac{1}{\tau_d(1)}, \tag{35}$$

where $z=1^{\pm}$ denotes values just above or below $z=1$. Note that while the interface conditions (33) and (34) are obtained by integrating (18) and (19), respectively, in z between 1^- and 1^+, the derivation of the interface condition (35) requires asymptotic analysis that will be given in section 7.

5. Relationship between the current and RS14 models

The majority of known Eulerian models for spray- or particle-laden atmospheric boundary layer flows use mixture-type approach (Barenblatt and Golitsyn 1974; Wamser and Lykossov 1995; Rastigejev et al. 2011; RS14) that does not fully account for the interphase momentum and TKE exchange. One such mixture-type E–ϵ has been developed in RS14. It takes into account the spray inertia effect and the suppression of turbulent energy due to the vertical transport of spray by the turbulent flow. Below we show that the RS14 model is a limiting case of light droplets (for which droplet relaxation time τ_d is much smaller than other characteristic hydrodynamic times) of the broader theoretical description that we present here and that incorporates an accurate account of the momentum and TKE exchange between air and spray. Note that other ocean spray models mentioned above are also developed for this case. Specifically, in this limit the parameters, variables, and coefficients approach the following values

$$\begin{aligned}&(\pi_{17},\pi_1,q_{ae})\to 0,\quad \mathbf{u}^r\to 0,\\ &(c_1,\tau_d)\to 1,\quad k_w\to k_a,\quad c_0\to\frac{1}{\sigma_0'}.\end{aligned} \tag{36}$$

In this limit the momentum conservation equations (17)–(19) reduce to

$$u_w=u_a,\quad k_a\rho\frac{du_a}{dz}=1,\quad \frac{d_{aw}s}{\pi_1}\frac{ds}{dz}+s=H_{z-1}. \tag{37}$$

The asymptotic momentum equations (37) and turbulence model equations (20) and (21) with $q_{ae}=0$ are identical to the corresponding governing equations used in RS14.

All known mixture-type models that employ momentum conservation equations (37) assume that droplets have the same horizontal speed as the air but slip with terminal speed a_0 relative to air in the vertical direction, that is $\langle|\mathbf{u}^r|\rangle=a_0$. This also means that π_1 should have a finite value in such models, which contradicts the asymptotic limit (36). Yet, despite this inconsistency such an assumption allows one to account for the spray mass flux balance. The expression for c_0 in this case takes the form

$$c_0=\frac{1}{\sigma_0'}\sqrt{\frac{2\alpha}{2\alpha+3\pi_1^2C_\beta}},\quad C_\beta=1.8. \tag{38}$$

In conclusion of this section, we also note that in the present multifluid model the quantity s_0 represents the intensity of the spray source located at the wave-crest level and it is not necessarily equal to the spray concentration at this location. In our previous publications (Rastigejev et al. 2011; RS14; Rastigejev and Suslov 2016, 2019) the mixture-type model corresponding to the asymptotic limit (36) was employed. In this limit spray concentration at the wave-crest level is equal to s_0. For this reason, in our past papers the scaled spray concentration at $z=1$ was always $s(1)=1$ while here its value varies depending on the choice of other problem parameters.

6. Mechanisms of turbulence suppression by spray droplets

The suppression of the turbulence intensity in a spray-laden airflow is caused by two different effects, TA and GL, that are due to the air–droplet interaction and the upward transport of spray against gravity by the turbulent flow, respectively. The TA and GL intensities are given in Eq. (22) by terms q_{ae} and p_{ag}, respectively. Substituting the expressions

$$\begin{aligned}q_{aw}-2e_a=2e_a(c_1-1)&=-\frac{2\pi_{17}\tau_de_a}{\pi_{17}\tau_d+\tau_{aw}'}\\ &\approx-\frac{4\pi_{17}\tau_d}{3\alpha^2k_pz},\\ \mathbf{u}^r\cdot\mathbf{u}^d&=-(w^d)^2,\end{aligned}$$

valid for $z>1$ into the expression for q_{ae} [see Eq. (22)] and taking into account that $w^d=\pi_1C_w$, where $C_w\sim 1$, and that $\pi_{17}\ll 1$, we obtain the estimate for the TA source

$$q_{ae}\approx-\pi_{18}\frac{s}{\tau_d}\left(\pi_1^2C_w^2+\pi_{17}\frac{4\tau_d}{3\alpha^2k_pz}\right). \tag{39}$$

Similarly, we obtain the estimate for GL source for $z>1$

$$p_{ag}=-\pi_{12}\frac{sw^d}{\rho}\approx-\pi_{12}\pi_1\frac{C_ws}{\rho}. \tag{40}$$

From (39) and (40) we evaluate the ratio of TA and GL intensities

$$\begin{aligned}R\equiv\frac{q_{ae}}{p_{ag}}&\approx\frac{\rho}{\tau_d}\left(C_w+\frac{\pi_{17}}{\pi_1^2}\frac{4\tau_d}{3\alpha^2k_pC_wz}\right)\\ &=\frac{\rho}{\tau_d}\left(C_w+\frac{4u_\star^3\tau_d}{3\alpha^2k_pC_wa_0gz_wz}\right).\end{aligned} \tag{41}$$

Note that $R\gtrsim 1$ because $\rho\sim 1$ and $\tau_d\sim 1$, which means that the TA effect is at least as strong as GL one for all values of parameters. At high altitudes $R\sim 1$. Thus, both TA and GM are expected to make comparable contributions into the TKE reduction there. However, in the vicinity of the wave-crest level ($z\sim 1$), the ratio R can be quite large reaching $R\sim 10$ for hurricane speeds $u_\star\sim 4\,\mathrm{m\,s^{-1}}$ and droplets with sizes smaller than 100 μm. Thus, the TA effect is expected to dominate over the GL one near wave crests.

7. Asymptotic analysis

Here we employ the method of matched asymptotic expansions (Van Dyke 1964; Nayfeh 2008) to derive approximate model solutions valid for small values of Stokes number $\pi_{17} \ll 1$. Formally, this limit corresponds to MABL laden with fine spray for which the droplet terminal velocity a_0 remains small. The droplet relaxation time required to reach this velocity is much smaller than the time scale of turbulent eddies. In practice, asymptotic solutions are expected to remain accurate for $\pi_{17} \lesssim 0.1 - 0.2$. However, the actual degree of their accuracy is problem-specific: for some cases the acceptable accuracy can be retained up to $\pi_{17} \lesssim 1$.

It follows from the definition of π_{17} that $a_0 = \pi_{17} g z_w / u_\star$. In turn, the droplet terminal velocity a_0 depends on the droplet radius r as described in Rastigejev and Suslov (2016, their appendix B). This enables us to compute the $\pi_{17} = \text{const.}$ contours in the $(u_\star, r)$ plane that are shown in Fig. 1. The asymptotic solutions derived here are expected to be accurate at least below the solid line in the figure.

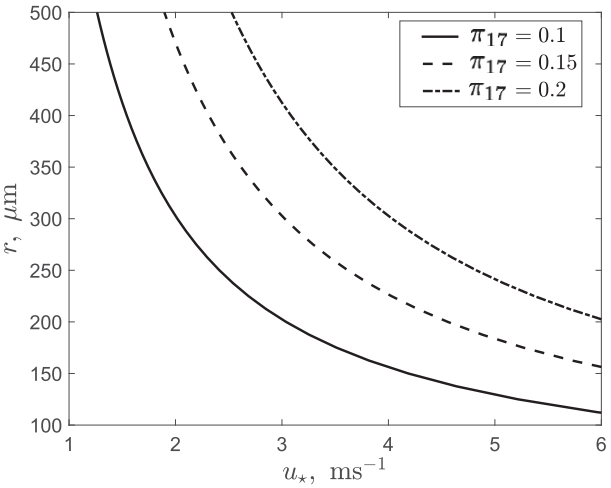

FIG. 1. The guaranteed validity region of asymptotic solutions is below the solid line.

If spray concentration s_0 is small, then TKE suppression due to gravity lubrication and turbulence attenuation by droplets slipping relative to surrounding air is negligible. Therefore, expressions for the nondimensional TKE, its dissipation rate, the characteristic turbulent time, and the turbulent viscosity coefficients are given by

$$e_a = \frac{1}{\alpha}, \quad \epsilon_a = \frac{1}{k_p z}, \quad \tau'_a = \frac{3}{2}\alpha k_p z, \quad k_a = k_p z. \tag{42}$$

We derive asymptotic solutions for the vertical distributions of spray concentration and its horizontal velocity next.

a. *Vertical spray distribution*

We start with deriving the boundary condition for spray momentum conservation equation (30) at the lower edge of the computational domain. Newton's second law of motion for spray droplets falling vertically with the ensemble-average droplet velocity, time and droplet relaxation time nondimensionalized as $\mathbf{w}_w = \tau_{d0} g \mathbf{w}_w$, $\tilde{t} = \tau_{d0} t$, and $\tilde{\tau}_d(z) = \tau_{d0}\tau_d(z)$, respectively, reads

$$\frac{d\mathbf{w}_w}{dt} + \frac{\mathbf{w}_w}{\tau_d(z)} + 1 = 0, \tag{43}$$

where the first term is the ensemble-average vertical droplet acceleration and the second and third terms are the negatives of the air–droplet ensemble-average drag and gravity forces per unit mass of a droplet, respectively. It is shown in section b of the appendix that $\tau_d(z)$ reaches its maximum at the location $z_{\max} = 1 - \eta_1$, where $\eta_1 = O(\sqrt{\pi_{17}}\ln\pi_{17})$. Hence, with high degree of accuracy it can be regarded as a constant in the vicinity of this maximum: $\tau_d(z) \approx \tau_d(1) \equiv \tau_{d1}$ over the vertical coordinate range $1 - \eta_1 < z < 1$. Therefore, here (43) becomes

$$\frac{d\mathbf{w}_w}{dt} + \frac{\mathbf{w}_w}{\tau_{d1}} + 1 = 0 \quad \text{and} \quad \mathbf{w}_w = (w_0 + \tau_{d1})\exp\left(-\frac{t}{\tau_{d1}}\right) - \tau_{d1}, \tag{44}$$

where w_0 is the initial ensemble-average vertical velocity component of droplets. Here we assume that w_0 is of the same order or smaller than the droplet terminal speed τ_{d1}, i.e., $|w_0| \lesssim \tau_{d1}$. It follows from (44) that below the wave-crest level droplets reach their local terminal speed $-\tau_{d1}$ at nondimensional time $t \sim \tau_{d1} \sim 1$ after traveling downward a nondimensional distance $\tau_{d1}\{t - (w_0 + \tau_{d1})[1 - \exp(-t/\tau_{d1})]\} \sim 1$. Note that here the length scale is defined as $\tau_{d0}^2 g$ in contrast to z_w used in (15). Thus, to express the distance η_2 traveled by a droplet downward before it reaches its terminal speed in terms of z_w we multiply its nondimensional value by the factor $\tau_{d0}^2 g / z_w$ to obtain $\eta_2 \sim \tau_{d0}^2 g / z_w = \pi_{17}\pi_1 \sim \pi_{17}$.

After reaching their terminal speed $-\tau_{d1}$ at $z \sim \eta_2$ droplets continue to travel with that terminal speed a distance $\eta_1 \gg \eta_2$, thus using the expression in the last line of (23) we obtain

$$\mathbf{w}_w = -\frac{1}{s} + \frac{d_w}{\pi_1}\frac{1}{s}\frac{ds}{dz} = -\tau_{d1}, \tag{45}$$

for $1 - \eta_1 \lesssim z \lesssim 1 - \eta_2$. Relationship (45) is adopted as the boundary condition for the spray momentum conservation equation (30) and is applied at $z = 1 - \eta_1$. Next, we substitute an (outer) asymptotic expansion

$$s^o(z) \sim s_0^o(z) + \pi_{17} s_1^o(z) + \cdots, \tag{46}$$

into (30) and collect terms involving similar powers of π_{17}. The equation

$$\frac{k_p z c_0}{\pi_1}\frac{ds_0^o}{dz} + \tau_d s_0^o - 1 = 0 \tag{47}$$

arising at the leading order has a general solution

$$s_0^o(z) = \frac{C_0}{F(1,z)} + \int_1^z \frac{\omega(\eta)F(z,\eta)}{\eta}\, d\eta, \tag{48}$$

where

$$F(a,b) = \exp\left[\int_a^b \frac{\omega(\eta)\tau_d(\eta)}{\eta}\, d\eta\right], \quad \omega(\eta) = \frac{\pi_1}{k_p c_0(\eta)},$$

and C_0 is the integration constant.

Note that for a limiting case of very small droplets $\pi_{17} \to 0$, which implies that $\tau_d(z) = \tau_{d1}$ and $c_0(z) = 1/\sigma_0^t$, Eq. (47) has a well-known solution $s = 1/\tau_{d1}$, corresponding to the case of droplets uniformly falling with a constant terminal speed $-\tau_{d1}$. By matching this solution with the form

$$s_0^o(z) = \frac{1}{\tau_{d1}} + z^{-\pi_1 \sigma_0^t \tau_{d1}/k_p}\left(C_0 - \frac{1}{\tau_{d1}}\right), \tag{49}$$

that (48) takes in this limiting case we obtain $C_0 = 1/\tau_{d1}$.

The (outer) solution (46) breaks down in the vicinity of $z = 1$, where a fast variation of quantities caused by the presence of a localized spray source occurs [this region is frequently referred to as "boundary layer" in mathematical literature dealing with perturbation methods (Nayfeh 2008), which should not be confused with physical MABL investigated here]. To overcome this difficulty, we introduce the stretched coordinate $\xi = (z - 1)/\pi_{17}$ and consider an (inner) solution

$$s^i(\xi) \sim s_0^i(\xi) + \pi_{17} s_1^i(\xi) + \cdots. \tag{50}$$

Then Eq. (30) and boundary conditions (35) and (45) become to the leading order

$$\frac{d}{d\xi}\left(\frac{4k_{w0}^i}{3}\frac{d\ln s_0^i}{d\xi}\right) - \frac{1}{\tau_{d0}^i}\frac{d_{aw0}^i}{\pi_1}\frac{ds_0^i}{d\xi} = 0, \tag{51}$$

$$\left.\frac{ds_0^i}{d\xi}\right|_{\xi \to -\infty} = 0, \quad \left.\frac{ds_0^i}{d\xi}\right|_{\xi = 0^-} = 0. \tag{52}$$

The solution of (51) subject to (52) is constant. Then the matching condition (Van Dyke 1964)

$$\lim_{z \to 1} s_0^o = \lim_{\xi \to -\infty} s_0^i$$

leads to $s_0^i = 1/\tau_{d1}$.

The leading-order composite asymptotic solution valid throughout the complete domain then is

$$s(z) \approx \frac{1}{\tau_{d1} F(1, z)} + \int_1^z \frac{\omega(\eta) F(z, \eta)}{\eta} d\eta. \tag{53}$$

By setting $z = 1$ in (53) we obtain interface boundary condition (35).

For small values of π_1 or $\omega(\eta) \ll 1$, which corresponds to strong winds and/or light droplets, solution (53) simplifies further and becomes

$$s(z) \approx \frac{1}{\tau_{d1}} + \int_1^z \frac{\omega(\eta)[1 - \tau_d(\eta)/\tau_{d1}]}{\eta} d\eta.$$

Since $\omega \ll 1$ in this case, the droplet concentration remains nearly constant below the wave-crest level, i.e., $s(z) \approx 1/\tau_{d1}$ even though $\tau_d(z)$, which is a nondimensional local terminal speed of a droplet, may vary with z.

For $z > 1$ the spray momentum conservation equation is given by (32) subject to boundary condition obtained by setting $\xi = 0$ in (50):

$$s(1) = \frac{1}{\tau_{d1}} + \pi_{17} s_1^i(0) + \cdots.$$

The leading-order asymptotic solution in this case is

$$s(z) \approx \frac{1}{\tau_{d1}} \exp\left[-\int_1^z \frac{\omega(\eta)\tau_d(\eta)}{\eta} d\eta\right]. \tag{54}$$

b. Horizontal spray velocity

If spray concentration is sufficiently small, its influence on the logarithmic air velocity profile is negligible. The expressions for the horizontal spray velocity obtained from the momentum conservation equations (29) and (31) subject to the interfacial and boundary conditions (33), (24), and (25). After substituting the outer asymptotic expansion for the horizontal spray velocity

$$u_w^o(z) \sim u_{w0}^o(z) + \pi_{17} u_{w1}^o(z) + \cdots, \tag{55}$$

into (29) and (31) and solving the equation at order of π_{17}^0, we obtain the leading-order outer solution

$$u_{w0}^o(z) = u_a(z) = \frac{1}{k_p}\ln\left(\frac{z}{z_0}\right). \tag{56}$$

Similar to the vertical spray distribution the outer solution for the horizontal spray velocity component breaks down in the vicinity of $z = 1$ and to overcome this problem we introduce coordinate stretching near $z = 1$, which, however, has a different scaling $\xi = (z - 1)/\sqrt{\pi_{17}}$. Equations (29) and (31) and the interfacial condition (33) transform into

$$\frac{d}{d\xi}\left(k_w s \frac{du_w^i}{d\xi}\right) + \sqrt{\pi_{17}}\pi_1 \frac{du_w^i}{d\xi} + s\frac{u_a - u_w^i}{\tau_d} = 0, \quad \xi < 0, \tag{57}$$

$$\frac{d}{d\xi}\left(k_w s \frac{du_w^i}{d\xi}\right) + s\frac{u_a - u_w^i}{\tau_d} = 0, \quad \xi > 0, \tag{58}$$

$$\left.\frac{du_w^i}{d\xi}\right|_{\xi = 0^-}^{\xi = 0^+} + \sqrt{\pi_{17}}\pi_1 \left.\frac{u - u_w^i}{k_w s}\right|_{\xi = 0} = 0. \tag{59}$$

Substituting the corresponding inner asymptotic expansion

$$u_w^i(\xi) \sim u_{w0}^i(\xi) + \sqrt{\pi_{17}} u_{w1}^i(\xi) + \cdots, \tag{60}$$

into (57)–(59) and matching the coefficients of like powers of π_{17} we obtain equations and interfacial conditions for individual ascending orders of a small parameter starting with zeroth (these equations for the zeroth- and first-order terms, $u_{w0}^i(\xi)$ and $u_{w1}^i(\xi)$, respectively, are given in section d of the appendix). After solving these equation and matching the inner and outer solutions we obtain the leading-order composite solution

$$u_w(z) \approx u_a(z) + \frac{\sqrt{\pi_{17}}\pi_1 \tau_{d1}^{3/2}[u - u_a(1)]}{2\sqrt{k_p \sigma_0^t c_{01}}} \times \exp\left[\frac{\pm(z - 1)}{\sqrt{k_p \pi_{17} \tau_{d1} \sigma_0^t c_{01}}}\right], \tag{61}$$

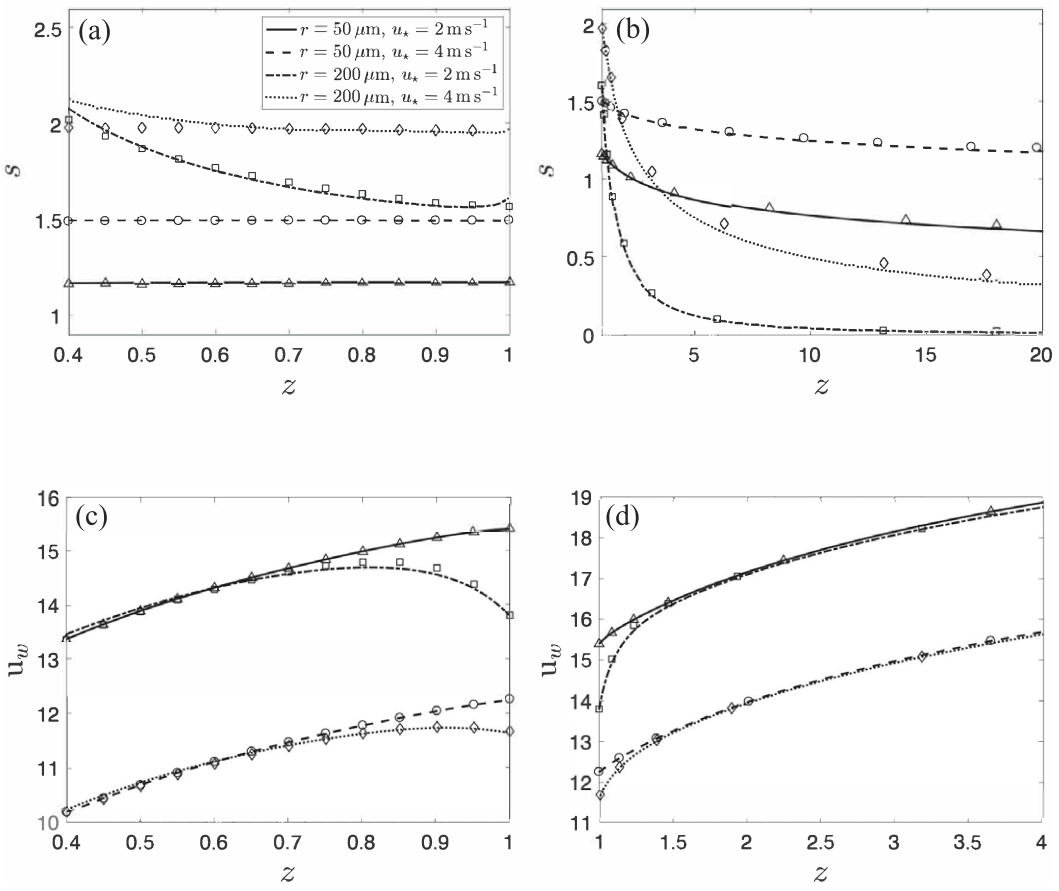

FIG. 2. Vertical distributions of the (a),(b) spray volume fraction s and (c),(d) horizontal spray velocity u_w for $s_0 = 10^{-5}$ and various values of droplet radius r and friction velocity $u_\star$. Shown are the (left) s and (right) u_w distributions below ($z < 1$) and above ($z > 1$) the wave-crest level. The lines and symbols depict asymptotic and numerical solutions, respectively.

where $c_{01} \equiv c_0(1)$. The plus and minus signs in (61) correspond to $z < 1$ and $z > 1$, respectively. Note that the leading-order approximation depends on the droplet relaxation time τ_{d1} at the wave-crest level, where the spray is produced, but it does not depend on the vertical distribution of $\tau_d(z)$. However, the higher-order approximations do depend on the vertical variation of the droplet relaxation time. Note that it follows from (61) that $u_w(z) \approx u_a(z)$ for $z \lesssim 1 - \sqrt{k_p \pi_{17} \tau_{d1} \sigma_0' c_{01}}$. Hence, relationship $\tilde{u}_w(z) = \tilde{u}_a(z)$ is adopted as the lower boundary condition (13).

8. Results

Similar to RS14, all results reported in this section are computed for parameters evaluated for $z_w = 5$ m and $z_{0c} = 0.4$. The model equations are solved numerically using a standard MATLAB boundary-value problem routine bvp5c. The computational grid is chosen automatically to achieve the prescribed absolute numerical tolerance of 10^{-5}. Equations for regions $z \lessgtr 1$ (see section 4) are solved separately with the intermediate boundary condition $u_w = A_u u_a$ at $z = 1$, where $0 < A_u < 1$ is a constant, the value of which is found iteratively to satisfy the interface condition (33). To reduce computational time and ensure the stability of convergence a parametric continuation is used when the output from one computational run is supplied as an initial guess for the next run with varied governing parameters. With such a strategy most of solutions are obtained within less than 2 min using a standard 6-core laptop computer with the Intel Core i7 processor.

a. *Asymptotic solutions*

To validate our numerical code and estimate the limits of validity of the developed asymptotic solutions we compare the numerical and asymptotic results for spray droplets of various radii and for various friction velocities in Fig. 2. The vertical profiles of several distributions are presented for regions below ($z < 1$) and above ($z > 1$) the wave-crest level. The upper (Figs. 2a,b) and lower (Figs. 3c,d) panels show asymptotic solutions (53) and (54) for the spray volume fraction and distributions (61) for the horizontal spray velocity, respectively.

For $z < 1$, the difference between the two sets of results for spray volume fraction distribution does not exceed 0.5% for small droplets with $r = 50\ \mu$m. For large droplets with $r = 200\ \mu$m the error increases but still does not exceed a few percent. A similar

trend is observed for the horizontal spray velocity component—the difference between the numerical and asymptotic results is ~0.04% for $r = 50\ \mu$m but it increases up to 1% for $r = 200\ \mu$m. Since the asymptotic solution for $z < 1$ is not valid for lower part of the domain, its deviation from the numerical solution increases at small z. This trend becomes more pronounced for large droplets.

For $z > 1$, the difference between the asymptotic and numerical distributions of spray volume fraction does not exceed 1% of its corresponding value at the wave-crest level for $r = 50\ \mu$m and 2%–3% for $r = 200\ \mu$m. The difference for the horizontal spray velocity component varies between ~0.02% for $r = 50\ \mu$m and 1% for $r = 200\ \mu$m. The increase in the difference between numerical and asymptotic solutions with the droplet radius is expected because the expansion parameter π_{17}, and thus the error of the asymptotic approximation, increases with the droplet size. The observed good agreement between asymptotic and numerical solutions the reliability of asymptotic expressions (53), (54), and (61) for droplets with radius as large as 200 μm.

b. Vertical spray distribution

Expressions (53) and (54) show that the vertical distribution of spray volume fraction predicted by the present model for small spray concentrations (when the TKE suppression effects due to spray presence are negligible) differs noticeably from

$$s(z) = \begin{cases} 1, & z \le 1, \\ z^{-\lambda_0}, & z > 1, \end{cases} \tag{62}$$

$$\lambda_0 = \frac{\pi_1 \sigma_0'}{k_p}\sqrt{1 + \frac{3C_\beta \pi_1^2}{2\alpha}}, \quad C_\beta = 1.8 \tag{63}$$

reported in RS14. Specifically, the present model predicts that the spray concentration $s(z)$ below the wave-crest level is nonuniform. It is 20%–50% higher than that predicted in RS14 for relatively small droplets with radius $r = 50\ \mu$m and about twice as high for large droplets $r = 200\ \mu$m (see Fig. 2). This discrepancy occurs because the present model accounts for the increase of the air–droplet drag and hence for the decrease in the droplet terminal speed τ_d in a turbulent flow. A slower downward motion of droplets in turn leads to their accumulation below the wave-crest level and the increase of their concentration $s \sim 1/\tau_d$ there.

For $z > 1$, we rewrite expression (54) for the vertical distribution of spray concentration in the form convenient for further analysis

$$s(z) = \frac{1}{\tau_{d1}}\exp\left[-\int_1^z \frac{\lambda(\eta)}{\eta}\,d\eta\right]. \tag{64}$$

Note that λ_0 and $\lambda(z)$ may differ noticeably (e.g., by a factor of 2 for $r = 200\ \mu$m) for the same values of the problem parameters. This occurs primarily because of the higher turbulent air–droplet drag taken into account by the present model compared to that in quiescent air. Computations reveal that $\lambda(z)$ monotonically increases or decreases with z and

$$\lambda_{\min} \le \lambda(z) \le \lambda_{\max}, \tag{65}$$

for $1 < z < z_\infty$. From (64) and (65) we obtain

$$\frac{z^{-\lambda_{\max}}}{\tau_{d1}} \le s(z) \le \frac{z^{-\lambda_{\min}}}{\tau_{d1}}. \tag{66}$$

Computational results also show that $\lambda_{\max} - \lambda_{\min} \lesssim 0.1\pi_1 \ll 1$ for droplets with radius $r \lesssim 200\ \mu$m. This means that the values of exponents of the bounding power functions are close. Thus, for droplets with radii $r \lesssim 200\ \mu$m the vertical distribution of spray concentration can be sufficiently accurately approximated by a power function. The error of such an approximation rapidly decreases with droplet's radius. Therefore, the vertical spray distribution above the wave-crest level for such droplets is still approximately described by a power law as in (62) with somewhat different scaling factors and exponents. However, for larger droplets the power function approximation may not be accurate.

c. TKE reduction due to the air–droplet slip

Figure 3 shows the comparative distributions of MABL characteristics obtained when the turbulence attenuation due to the air–droplet interaction is absent ($q_{ae} = 0$) and present ($q_{ae} \neq 0$) in Eqs. (20) and (21) for fine- ($r = 50\ \mu$m) and large-droplet ($r = 200\ \mu$m) spray with source intensity $s_0 = 10^{-4}$ and friction velocity $u_\star = 4\ \mathrm{m\ s^{-1}}$. The figure demonstrates a very strong turbulence suppression by the air–droplet interaction that in turn leads to a significant reduction of turbulent viscosity and, subsequently, to the airflow acceleration, see the solid and dashed lines in Figs. 3d, 3e, and 3a, respectively. In contrast, when TA due to air–droplet interaction is removed from the turbulence model by prescribing $q_{ae} = 0$, the TKE suppression due to vertical transport of the spray against the gravity is substantially weaker so that the turbulent viscosity and air velocity profiles remain close to the distributions given by the standard spray-free E–ϵ model, see the dash–dotted and dotted lines in the same panels. When $q_{ae} \neq 0$, Fig. 3d shows that TKE reaches its minimum value $e_{a\min} \approx 2.16$ at $z \approx 2.64$ and $e_{a\min} \approx 2.26$ at $z \approx 2.56$ for droplets with $r = 50$ and 200 μm, respectively. The corresponding TKE values at the same locations computed by setting $q_{ae} = 0$ (the dash–dotted and dotted lines in Fig. 3d) are $e_a \approx 3.23$ and 3.06. Therefore, suppression due to TA given by the difference $e_a - e_{a\min}$ is much stronger than that due to GL that is characterized by $\alpha - e_a$. Indeed,

$$\frac{e_a - e_{a\min}}{\alpha - e_a} \approx 10.3 \text{ and } 2.9,$$

for droplets with $r = 50$ and 200 μm, respectively, the result consistent with estimates (41). This ratio reduces with z (see Fig. 3c) consistently with (41).

Remarkably, the turbulence suppression and airflow acceleration due to the spray presence observed for nonzero TA remain strong even though the concentration of spray, which is known to lead to such an effect according to the mixture-type model RS14, reduces with the altitude much faster when $q_{ae} \neq 0$, see Fig. 3c. This demonstrates that turbulence attenuation due to air–droplet interaction plays the major role in defining the dynamics of MABL. Figure 3b shows the vertical distribution of the horizontal spray velocity component u_w. For all cases u_w is a few percent smaller than that of the airflow u_a around $z = 1$ due to the difference between the velocity u of injected droplets and that of airflow (in these calculations the droplet injection velocity is taken to be zero). However, droplet velocity approaches that of the air short distance $\sim\sqrt{k_p \pi_{17} \tau_{d1} \sigma_0' c_{01}}$ [see (61)] away from wave crests.

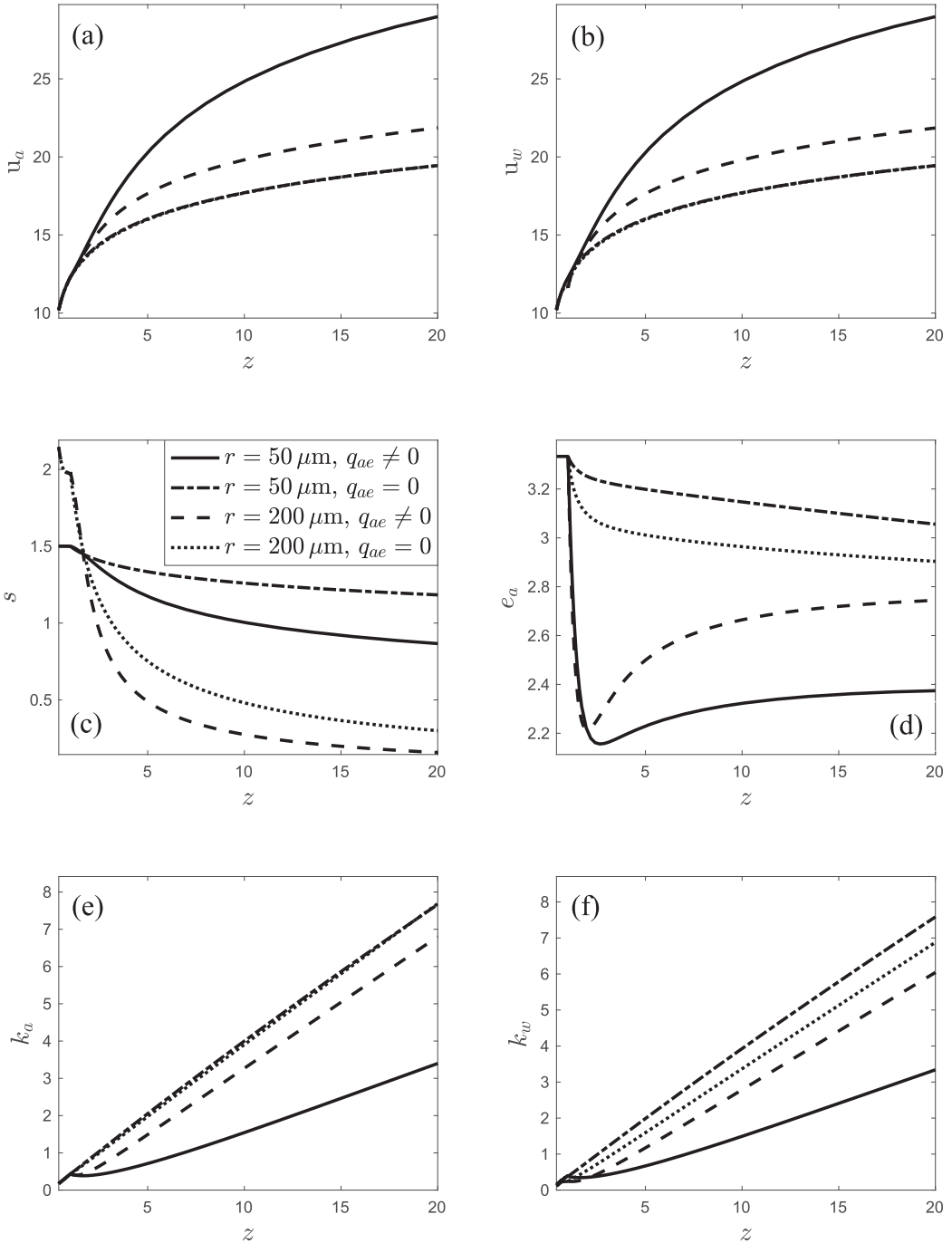

FIG. 3. Vertical distributions of MABL quantities: (a) airspeed, (b) average spray droplet speed, (c) spray concentration, (d) turbulent kinetic energy, (e) turbulent viscosity of air, and (f) turbulent viscosity of droplets for $u_\star = 4\,\text{m s}^{-1}$ with ($q_{ae} \neq 0$) and without ($q_{ae} = 0$) turbulence attenuation caused by air–droplet interaction for 50 and 200 μm spray droplets. Spray source intensity $s_0 = 10^{-4}$ for all computations. The two $q_{ae} = 0$ curves are visually indistinguishable at the plot scale in (a) and (b). In (a) they also overlap with the reference logarithmic velocity profile for spray-free air.

Figure 3f shows that the distribution of the turbulent viscosity k_w of spray generally follows the same trends as those for the air k_a (cf. with Fig. 3e), but as intuitively expected the sensitivity of k_w to the droplet size is more pronounced than that of k_a. The plots show that the vertical turbulent transport is considerably weaker in the TA case $q_{ae} \neq 0$.

Figure 4 demonstrates the vertical distribution of TKE in several representative regimes. Consistently with the conclusions

made in RS14 using a simpler model, we observe that fine spray permanently suppresses turbulence throughout MABL, see the solid line, while large-droplet spray suppresses TKE mostly near the wave-crest level: the dash–dotted line indicates gradual recovery of TKE at high altitudes, where the concentration of heavy droplets is close to zero, see the dashed line in Fig. 3c. The transition between the two regimes occurs when the value of parameter λ_0 defined by (63) approaches 1, see the dashed line in Fig. 4. Also, note that when the turbulence intensity characterized by $u_\star$ and the associated turbulent diffusion increase, more spray droplets reach higher altitudes leading to greater turbulence attenuation there. Therefore, the increase of MABL turbulence caused by high-altitude driving processes (parameterized by $u_\star$) also leads to its stronger relative suppression in MABL, compare the dashed and dash–dotted curves in Fig. 4.

In Fig. 5 we show the distributions of spray concentration $\tilde{s}$ at the wave-crest level $\tilde{z}_w$ and of the drag coefficient $C_d = 1/(u_{a10}^2 + \sigma s_0 s u_{w10}^2)$ 10 m above the average sea level. In our current model the friction velocity $u_\star$ and the spray source intensity s_0 are taken as independent governing parameters. Since the meaning of s_0 here is different from the spray concentration at the wave-crest level that we used in our previous publications (Rastigejev et al. 2011; RS14; Rastigejev and Suslov 2016), to enable a meaningful comparison mapping $(s_0, u_\star) \to \tilde{s}(\tilde{z}_w)$ is computed and shown in Fig. 5a by the labeled contour lines. It shows that the spray concentration at the wave-crest level increases with both the spray source intensity s_0 and the friction velocity $u_\star$ [the thin solid contour lines representing the constant values of $\tilde{s}(\tilde{z}_w)$ slope down at larger values of $u_\star$], which is due to the facts that $\tilde{s} \sim s_0/\tau_d$ and that τ_d decreases with $u_\star$ according to (23) and (A11). The dependence of drag coefficient C_d on s_0 and $u_\star$ is shown in Fig. 5c by labeled contour lines. It increases with $u_\star$ (from left to right in the figure) but decreases with s_0 (the constant C_d contours have positive slopes). When considered as a function of $\tilde{u}_{10}$, as seen from Fig. 5d the variation of the drag coefficient is nonmonotonic and depends on the path in the $(s_0, u_\star)$ plane. Several correlations relating the spray concentration at the wave-crest level and the airspeed have been reported in literature. Here we consider the exponential and power law relations suggested in Andreas (1998) and Fairall et al. (2009), respectively. The former is given by

$$\tilde{s}(\tilde{z}_w) = A \exp\big[\delta(u_{a10} - u_r)\big], \tag{67}$$

where $A = 2 \times 10^{-7}$, $\delta = 0.2 - 0.6$ s m^{-1} and $u_r = 22$ m s^{-1}, while the latter reads

$$\tilde{s}(\tilde{z}_w) = A_n u_\star^n . \tag{68}$$

The mappings of these correlations for the typical values of $\delta = 0.2$ and 0.3 s m^{-1} (RS14) and $n = 3$ and $A_3 = 3.9 \times 10^{-6}$ s^3 m^{-3} (Rastigejev and Suslov 2019) in the $(s_0, u_\star)$ plane are shown in Figs. 5a and 5c by the thick solid, dashed, and dash–dotted lines, respectively. The corresponding variation of the wave-crest spray concentration $\tilde{s}$ and the drag coefficient C_d along these lines are shown in Figs. 5b and 5d, respectively, as functions of velocity $\tilde{u}_{10}$ registered 10 m above the mean sea level. As expected, the values of the spray concentration

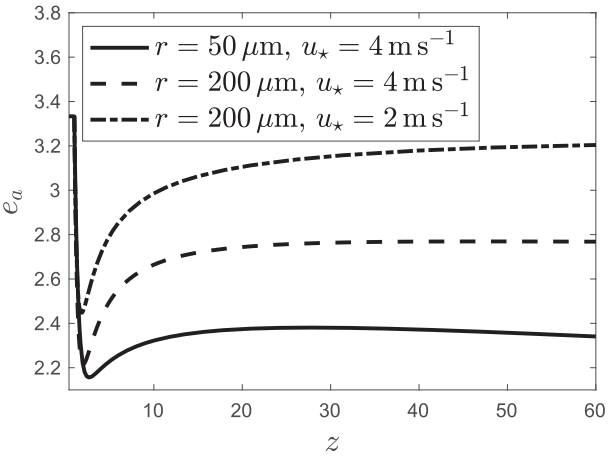

FIG. 4. The vertical distributions of nondimensional turbulent kinetic energy e_a for $s_0 = 10^{-4}$ and various droplet sizes and friction velocities. The estimated values of parameter λ_0 defined by (63) are 0.09, 0.99, and 3.28 for the distributions shown by the solid, dashed, and dash–dotted lines, respectively.

increase monotonically (see Fig. 5b) and this increase is steeper for larger values of δ. Yet, the values of the wave-crest concentration corresponding to maximum value of the drag coefficient $\tilde{s}_{\max}$ do not exceed 7×10^{-5} and 1.4×10^{-4} for exponential and power laws, respectively, which remains in the plausible range. However, even at the modest spray concentration values $\sim 10^{-5}$ a significant deviation of the drag coefficient behavior from that shown by the dotted line for spray-free atmosphere with the logarithmic velocity profile is observed (see Fig. 5d). Such a behavior of the drag coefficient (reaching the maximum and then starting to decrease with u_{10}) has been observed in various field and laboratory measurements (Donelan et al. 2004; Powell et al. 2003; Black et al. 2007; Haus et al. 2010; Zhao and Li 2019; Sun et al. 2021). It signals a strong influence of spray on the acceleration of air due to turbulence suppression. Our computations with $q_{ae} = 0$ show that in this case all C_d curves collapse onto the reference dotted line demonstrating that the TA effect is primarily responsible for the increase in the predicted wind speed. It is noteworthy that the deviation of C_d from the reference value was predicted by our previous modeling reported in RS14 but it was detected at an order of magnitude higher spray concentration $\sim 10^{-4}$. The main difference between our previous and current models is that here we take into account the turbulence attenuation due to spray slip relative to the surrounding air. Therefore, we confirm once again that such an effect plays a major role in the air–spray interaction in MABL.

In Fig. 6 similar distributions to those in Fig. 5 are shown but for much larger spray droplets. The figure reveals similar trends as for smaller droplets but the values of spray concentrations $\tilde{s}_{\max}$ corresponding to the maximum value of the drag coefficient C_d are somewhat higher, 1.0×10^{-4} and 1.8×10^{-4} for exponential and power laws, respectively. The maximum values of the drag coefficient are also larger by 4–5 and 10% than those for smaller droplets for exponential and power laws, respectively. At the first glance this observation

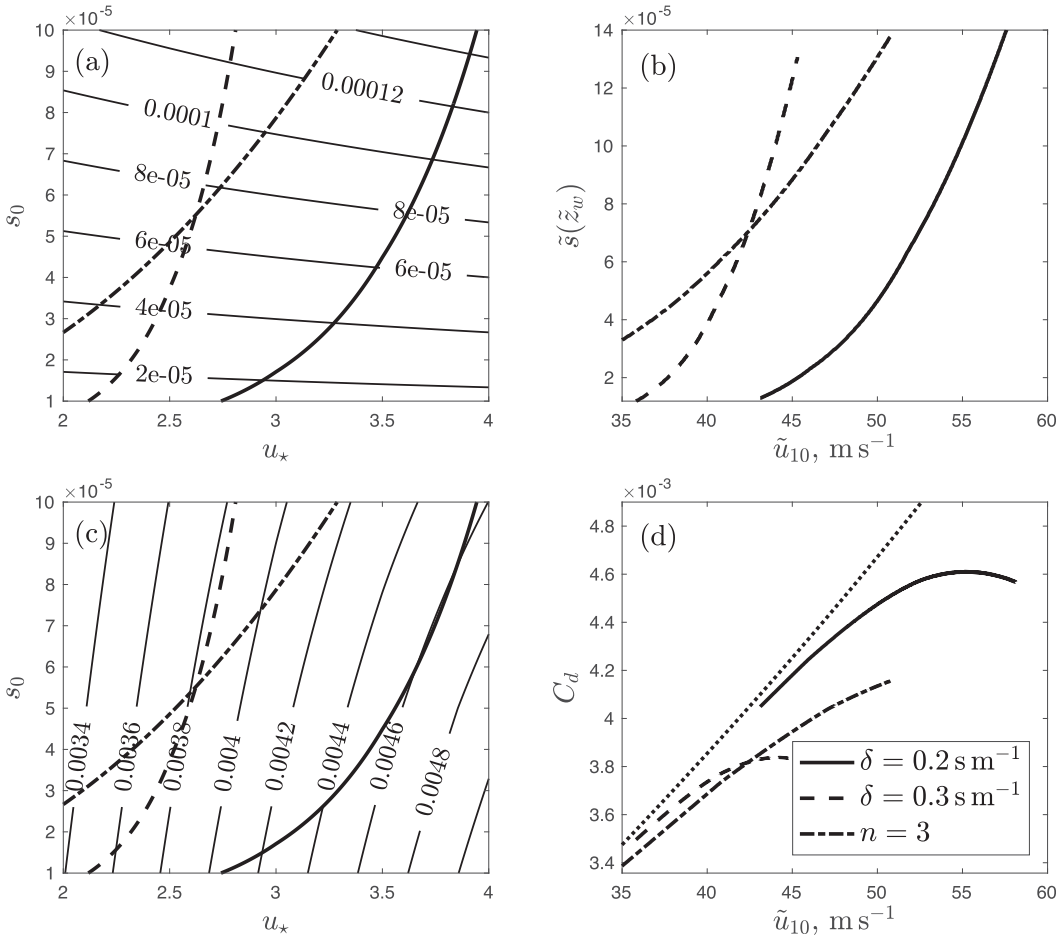

FIG. 5. Distributions of (a) spray concentration $\tilde{s}(\tilde{z}_w)$ at the wave-crest level and (c) of the drag coefficient C_d as functions of the friction velocity $u_\star$ and spray source intensity s_0; (b),(d) the same quantities as functions of the speed at the 10-m level assuming the exponential and power law correlation between $\tilde{s}(\tilde{z})$ and $u_\star$ (Andreas 1998; Fairall et al. 2009) mapped as shown by the thick solid, dashed, and dash–dotted lines in (a) and (c) for the average droplet radius $r = 50$ μm.

appears to be counterintuitive since spray slip relative to the surrounding air is not as pronounced for small droplets. Therefore, turbulence attenuation is stronger for large droplets. However, this is offset by their smaller concentration above the wave-crest level for the same s_0 compared with that of smaller droplets (see Fig. 3c). As a result of that, large droplets lead to a weaker turbulence suppression at high altitudes, and the flow laden with such droplets is characterized by a larger drag coefficient.

Figure 7 demonstrates that the drag coefficient dependence on the wind speed varies with the elevation above the sea level. Regardless of the used form of a spray–production correlation, the drag coefficient deviates from its reference values faster at higher altitudes. The value of $\tilde{u}_{10}$ at which the maximum of C_d is detected also shifts toward lower values with altitude. Such an altitude dependence of the drag coefficient has been detected and reported previously in RS14 and the more complete current model that takes into account spray slip relative to the air confirms this general conclusion.

The dependence of the drag coefficient on the altitude for droplets of various radii compared to the variation of the reference drag coefficient for spray-free atmosphere characterized by the logarithmic wind speed profile is shown in Fig. 8. The behavior of C_d for spray-laden atmosphere follows the reference one only for the first few meters above the wave crests. Starting from about 8 m above the average sea level the C_d values for spray-laden flows noticeably decrease relative the reference distribution due to the turbulence suppression caused by spray. Such an effect is stronger for fine spray that is carried by the turbulent eddies to higher altitudes. Again, this is consistent with findings reported in RS14.

9. Discussion and conclusions

We have developed a multifluid model of spray-laden MABL that considers air and dispersed in it sea spray droplets as two different interacting phases that generally have

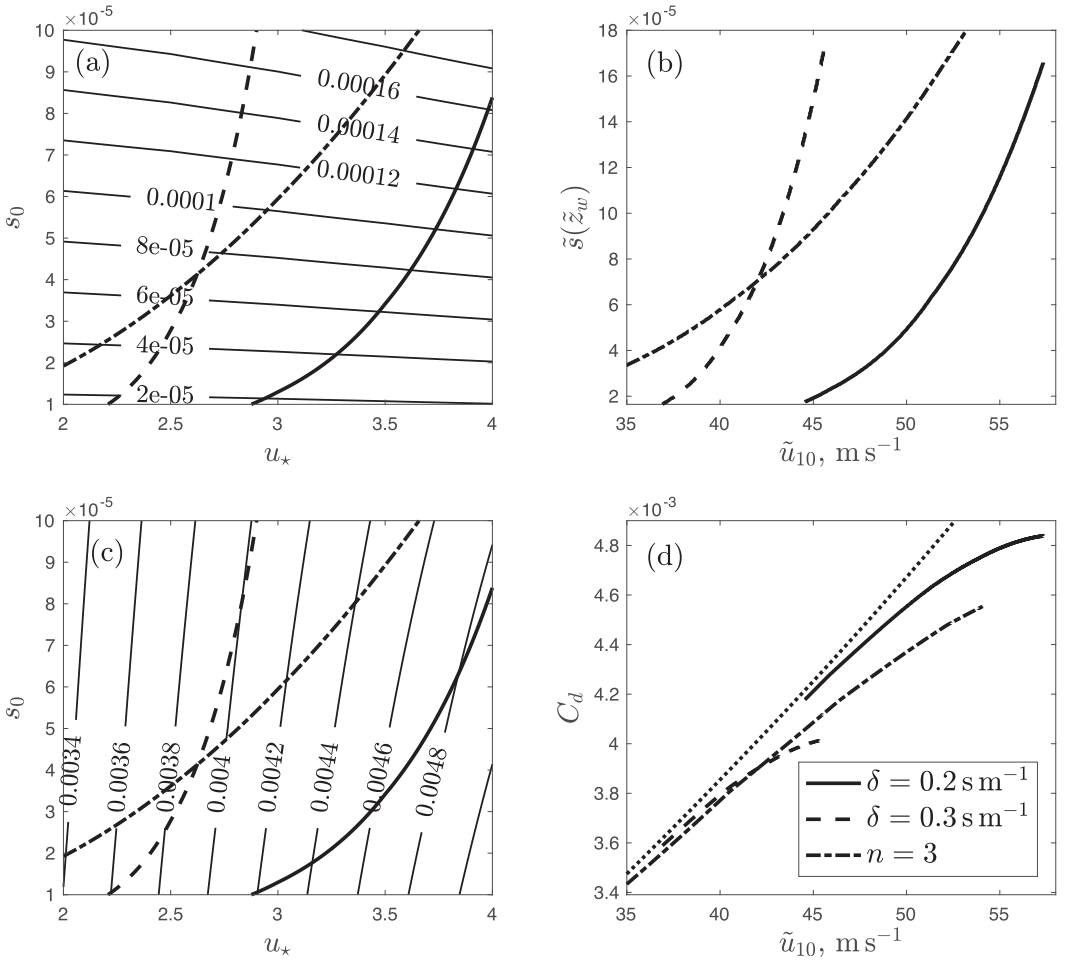

FIG. 6. As in Fig. 5, but for $r = 200\ \mu$m.

different velocities and can slip relative to each other. This is particularly so near the wave-crest levels, where the spray droplets are generated. The multifluid model enables us to consistently take into account the accelerating and decelerating influences of ocean spray due to its turbulence suppression effect and inertia, respectively. Subsequently, we carried out numerical and asymptotic analyses of the structure and dynamics of a MABL under high-wind conditions of a hurricane. Under such conditions the ocean spray is primarily generated by strong wind ripping off the droplets from the wave crests. It has been found that both the TA and GL effects make comparable contributions to turbulence dissipation for low wind speeds and large droplets. However, TA dominates by an order of magnitude or more for large wind speeds and small droplets. Remarkably, while the GL effect has been studied closely by several authors, the stronger TA effect that is primarily responsible for flow acceleration has not received the due attention to date. This is not surprising considering that GL can be sufficiently accurately described by a simple one-equation turbulence model or a model based on Monin–Obukhov similarity (Rastigejev et al. 2011) within a framework of the mixture-type approach, while a meaningful description of TA requires a much more complicated multifluid consideration coupled with a higher-order turbulence model.

The conclusions regarding the mechanical effect of spray on MABL made based on our previous mixture-type model reported in RS14 are qualitatively consistent with those of the current multifluid model, particularly so in the limiting case of light droplets. However, when droplet slip becomes significant, the two models have produced noticeably different results. In particular, our calculations show that spray droplets characterized by large values of parameter $\lambda_0 \sim a_0/u_\star \gtrsim 1$, where a_0 and $u_\star$ are the terminal droplet and friction velocities, respectively, tend to remain in a thin layer near the ocean surface and cause stronger suppression of turbulence there than that predicted by the mixture model of RS14. However, at higher elevations that cannot be reached by heavy droplets TKE tends to recover in a way consistent with that described in RS14. Small droplets with $\lambda_0 \lesssim 1$ are carried by the turbulent flow to higher altitudes permanently suppressing turbulence there. This is fully consistent with conclusions of RS14, however, with quantitatively much stronger turbulence reduction than that reported in RS14.

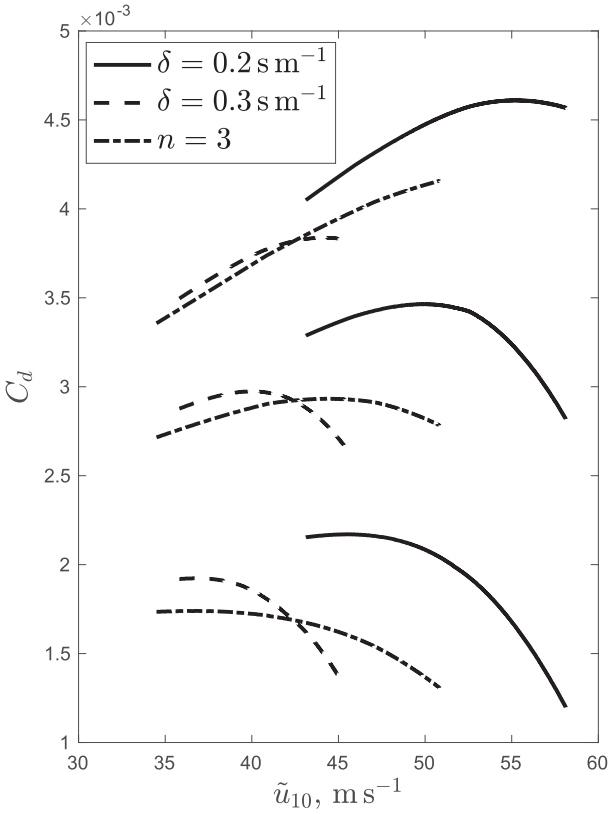

FIG. 7. The drag coefficient C_d for spray containing $r = 50$ μm droplets as a function of the horizontal wind speed at the 10 m level for the exponential and power law correlation between $\tilde{s}(\tilde{z})$ and $u_\star$. The data are presented (from top to bottom) for $\tilde{z} = 10$, 20, and 100 m.

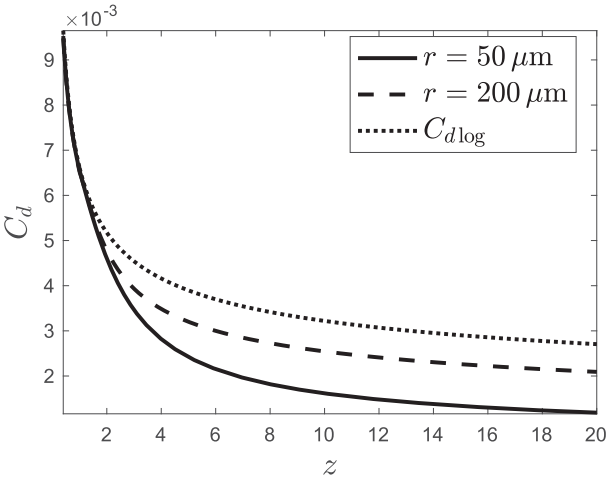

FIG. 8. The drag coefficient C_d for spray containing $r = 50$ and 200 μm droplets as a function of altitude z for $s_0 = 10^{-4}$ and $u_\star = 4\,\mathrm{m\,s^{-1}}$. The reference distribution $C_{d\log} = 1/u_{\log}^2 = k_p^2/\ln^2(z/z_0)$ for the spray-free atmosphere is shown by the dotted line.

Both RS14 and the current multifluid models corroborate that the mechanical effect of spray on the airflow is highly nonuniform in the vertical direction. This is because such an influence is determined by the balance between spray inertia and TKE suppression that vary dissimilarly with the altitude. The effect of droplet inertia is strong near the ocean surface, where spray is injected into MABL with a small velocity compared to the local wind speed. In the mixture model of RS14, the air and spray velocities are taken to be the same. Therefore, the inertia of slow-moving droplets dominates over the spray lubrication (turbulence suppression) effect near the bottom of MABL and the wind speed predicted there by RS14 is noticeably smaller than that of the reference logarithmic profile. The current multifluid model treats the momentum exchange process between air and spray droplets in this region much more realistically. According to it both the spray inertia effect on the wind and the lubrication effect due to the enhanced TKE suppression caused by TA are stronger compared to those predicted by the mixture model. Near the wave-crest level the two effects compensate each other. Therefore, the air velocity predicted by the multifluid model remains almost unchanged there compared to the reference logarithmic profile. However, a few meters above wave crests the spray lubrication dominates and the airflow accelerates.

Another important observation is that the multifluid model predicts noticeable wind acceleration and the corresponding reduction of the drag coefficient from the reference values for a spray-free atmosphere at spray volume fraction $\sim 10^{-5}$, which is an order of magnitude lower than the similar value predicted by the mixture model. The falloff of the drag coefficient from its reference values becomes quicker for higher spray concentrations and is stronger pronounced at higher altitudes. The drag coefficient reaches its maximum at spray volume fraction $\sim 10^{-4}$ that is several times smaller than the mixture model prediction.

To conclude, while both mixture-type model of RS14 and the current multifluid model are designed to quantify the mechanical effect of sea spray on the tropical cyclone dynamics, the latter provides a more accurate account of interphase momentum and TKE exchange in the air–spray turbulent flow. This produces quantitative difference between the results produced by the two models that is attributed to the influence of inertial droplet slip that is not captured by mixture-type models.

Finally, we note that the uniformity of the local distribution of heavy particles in vortical flows can be disrupted by centrifuge effects. A combination of asymptotic and numerical methods has been used to investigate such a swirl effect in the past (e.g., Druzhinin 1995a,b) but no attempt to take it into account was made in the current study. It was argued by Eaton and Fessler (1994) that particle clustering in swirling flows remains weak for particles characterized by small Stokes numbers (π_{17}) such as fine sea spray droplets considered here. However, large droplets that are also generated during hurricanes may still be affected. Investigation of the effect of such large droplet clustering may be a logical continuation of the current study.

Acknowledgments. The authors acknowledge support from the U.S. National Science Foundation via Award AGS-1832089.

APPENDIX

Equations and Asymptotic Expressions

a. Derivation of the governing equations

Below we use bars ($\bar{\cdot}$) and hats ($\hat{\cdot}$) for ensemble and mass-weighted averages, primes ($\cdot'$) and double primes ($\cdot''$) for turbulent fluctuations about ensemble and mass-weighted average values, respectively, and tildes ($\tilde{\cdot}$) for other dimensional variables. We assume that the average volume fraction of spray (also referred to as spray concentration) $\bar{s}$ is much smaller than that of air $1-\bar{s}$, i.e., $\bar{s} \ll 1$. This implies that the mass-weighted average of the air velocity is equal to its ensemble average $\hat{\mathbf{u}}_a = \bar{\mathbf{u}}_a$. Consequently, $\mathbf{u}_a'' = \mathbf{u}_a'$.

1) Continuity equation

The averaged continuity equations for air and spray are

$$\frac{\partial}{\partial \tilde{x}_k}(\bar{\rho}_a \bar{u}_{ak}) = 0\,, \tag{A1}$$

$$\frac{\partial}{\partial \tilde{x}_k}(\bar{s}\hat{u}_{wk}) = \bar{\dot{q}}_{1,w}\,, \tag{A2}$$

where $\bar{s}$, $\bar{\rho}_a$, $\bar{u}_{ak}$, $\hat{u}_{wk}$, and $\bar{\dot{q}}_{1,w}$ are the average volume fraction of spray, the mass density of air, the kth components of air and spray velocities, and the rate of production of spray per unit mass due to spume breakup, respectively. The mass-weighted average spray velocity $\hat{u}_{wk}$ is defined as

$$\hat{u}_{wk} = \frac{\overline{s u_{wk}}}{\bar{s}} = \bar{u}_{wk} + \frac{\overline{s' u'_{wk}}}{\bar{s}}.$$

Here and below repeated indexes follow the Einstein summation convention.

2) Momentum equations

The averaged momentum equations for air and spray read (Jakobsen 2008)

$$\begin{aligned}\bar{\rho}_a \bar{u}_{al}\frac{\partial \bar{u}_{ak}}{\partial \tilde{x}_l} = &-\frac{\partial \bar{p}}{\partial \tilde{x}_k} + \frac{\partial}{\partial \tilde{x}_l}\left\{\bar{\rho}_a\left[\tilde{k}_a\left(\frac{\partial \bar{u}_{ak}}{\partial \tilde{x}_l} + \frac{\partial \bar{u}_{al}}{\partial \tilde{x}_k}\right)\right]\right\} \\ &-\frac{2}{3}\frac{\partial}{\partial \tilde{x}_k}\left[\tilde{\rho}_a\left(\tilde{e}_a + \tilde{k}_a\frac{\partial \bar{u}_{al}}{\partial \tilde{x}_l}\right)\right] + \bar{\rho}_a g_k + \rho_w \bar{F}_k,\end{aligned} \tag{A3}$$

$$\begin{aligned}\bar{s}\hat{u}_{wl}\frac{\partial \hat{u}_{wk}}{\partial \tilde{x}_l} = &-\frac{1}{\rho_w}\overline{s\frac{\partial p}{\partial \tilde{x}_k}} + \frac{\partial}{\partial \tilde{x}_l}\left[\tilde{k}_w \bar{s}\left(\frac{\partial \hat{u}_{wk}}{\partial \tilde{x}_l} + \frac{\partial \hat{u}_{wl}}{\partial \tilde{x}_k}\right)\right] \\ &-\frac{2}{3}\frac{\partial}{\partial \tilde{x}_k}\left[\bar{s}\left(\tilde{e}_w + \tilde{k}_w\frac{\partial \hat{u}_{wl}}{\partial \tilde{x}_l}\right)\right] + \bar{s}g_k - \bar{F}_k \\ &+ (U_k - \hat{u}_{wk})\bar{\dot{q}}_{1,w},\end{aligned} \tag{A4}$$

where p, g_k, $\tilde{k}_a$, and $\tilde{k}_w$ are the pressure, the gravity acceleration, and the turbulent viscosity coefficients in air and spray, respectively. Note that the pressure term in Eq. (A4) is usually negligibly small because of the large water–air density ratio, but we keep it for completeness. The kth components of the average air–droplet interaction force $\bar{F}_k$, the average local relative interphase $\hat{u}_k^r$ and drift $\tilde{u}_k^d$ velocities are given by

$$\bar{F}_k = \frac{\bar{s}\hat{u}_k^r}{\tilde{\tau}_d}, \quad \hat{u}_k^r = \hat{u}_{wk} - \frac{\overline{s u_{ak}}}{\bar{s}} = \hat{u}_{wk} - \bar{u}_{ak} - \tilde{u}_k^d,$$

$$\tilde{u}_k^d = \frac{\overline{s u_{ak}}}{\bar{s}} - \bar{u}_{ak} = \frac{\overline{s' u'_{ak}}}{\bar{s}}\,.$$

Here a conventional closure model of the Reynolds stresses based on the eddy-viscosity hypothesis, also known as the Boussinesq hypothesis (Boussinesq 1897), has been adopted for both air and spray. This hypothesis assumes a linear relationship between the Reynolds stress and the average strain rate. Such an approach may potentially yield an inaccurate description of complex turbulent flows (e.g., flows with a sudden change in the mean strain rate, flows over curved surfaces or in rotating fluids, etc.). However, it produces satisfactory results for simple shear turbulent flows (Wilcox 2006) similar to the one considered in this study.

3) Marine atmospheric boundary layer flow

For the MABL flow that is homogeneous in the horizontal directions, the expressions for horizontal spray and vertical air velocities take the forms

$$\hat{u}_w = \bar{u}_w + \frac{\overline{u'_w s'}}{\bar{s}} = \bar{u}_w, \quad \bar{w}_a = 0,$$

and the average spray production source is

$$\bar{\dot{q}}_{1,w} = q_0 \tilde{\delta}_{\tilde{z}-z_w}\,, \tag{A5}$$

where $\tilde{\delta}_{\tilde{z}-z_w}$ is some suitably defined distribution function with a sharp maximum at $\tilde{z} = z_w$. Expressing q_0 using the characteristic value of the spray volume fraction $s_0 \equiv q_0/a_0$ and substituting (A5) into (A2) yields

$$\frac{d}{d\tilde{z}}(\bar{s}\hat{w}_w) = a_0 s_0 \tilde{\delta}_{\tilde{z}-z_w}, \tag{A6}$$

where a_0 is the terminal speed of spray droplets in quiescent air and

$$\hat{w}_w = \bar{w}_w + \frac{\overline{w'_w s'}}{\bar{s}} \equiv \bar{\mathbf{w}}_w + \frac{\overline{w'_w s'}}{\bar{s}} \tag{A7}$$

(for future convenience, here we introduced a different notation for the ensemble-average vertical spray velocity $\bar{\mathbf{w}}_w \equiv \bar{w}_w$). After integrating the spray continuity equation (A6) with respect to $\tilde{z}$ we obtain

$$\bar{s}\hat{w}_w = -a_0 s_0 \tilde{H}_{\tilde{z}-z_w}, \quad \tilde{H}_{\tilde{z}-z_w} = \int_{\tilde{z}-z_w}^{\infty} \tilde{\delta}_\xi\, d\xi.$$

b. Approximate expression for droplet relaxation time τ_d

Here we derive an approximate expression for the nondimensional droplet relaxation time $\tau_d(z)$ for light droplets

characterized by $\pi_{17} \ll 1$. It follows from (23) that τ_d depends only on the RMS of relative velocity $\langle|\tilde{\mathbf{u}}^r|\rangle$ defined by (11). The vertical component of the relative velocity can be expressed in terms of w_w and $\mathfrak{w}_w$ [defined by (15)] as follows

$$\begin{aligned} w^r &= \pi_1 w_w - w^d = \pi_1 w_w - c_1 w^f \\ &= \pi_1 w_w - c_1 \pi_1 (w_w - \mathfrak{w}_w) \\ &= \pi_1 \big[(1-c_1) w_w + c_1 \mathfrak{w}_w\big]. \end{aligned} \tag{A8}$$

Substituting the expression (16) for w_w into (A8) and taking into account that $\mathfrak{w}_w \approx -\tau_d$ for $\pi_{17} \ll 1$ we obtain

$$w^r \approx \pi_1 \left[(c_1 - 1)\frac{H_{z-1}}{s} - c_1 \tau_d\right]. \tag{A9}$$

Substituting (A9) into (11) we obtain the following expression for the RMS of relative velocity

$$\begin{aligned} \langle|\mathbf{u}^r|\rangle \approx \Bigg\{ &\left[(c_1 - 1)\frac{H_{z-1}}{s} - c_1 \tau_d\right]^2 \pi_1^2 \\ &+ (u_a - u_w)^2 + 2e_a(1 - c_1)\Bigg\}^{1/2}. \end{aligned} \tag{A10}$$

Substituting estimations $\tau_d(z) \approx \tau_{d1}$ for the particle relaxation time and $s(z) \approx 1/\tau_{d1}$ for the spray concentration below the wave-crest level and

$$c_1 \approx \frac{3\alpha k_p z}{2\pi_{17}\tau_{d1}\sigma_0' + 3\alpha k_p z}$$

obtained from (10) and (42) into (A10) yields

$$\langle|\mathbf{u}^r|\rangle \approx \left[(c_2 \tau_{d1} \pi_1)^2 + (u_a - u_w)^2 + \frac{4\pi_{17}\tau_{d1}\sigma_0'}{\alpha(2\pi_{17}\tau_{d1}\sigma_0' + 3\alpha k_p z)}\right]^{1/2}, \tag{A11}$$

where $c_2 = 1$ for $z < 1$ and $c_2 = c_1$ for $z \geq 1$. The difference $u_a - u_w$ is evaluated using (61).

c. Maximum of $\tau_d(z)$ for $z < 1$

Below we prove that when $\pi_{17} \ll 1$, $\tau_d(z)$ always has a single maximum at some location $z_{\max}$ below the wave-crest level $z < 1$ where $d\tau_d/dz = 0$. This results in the equation for $z_{\max}$

$$\exp\left(\frac{z_{\max} - 1}{\sqrt{\pi_{17}} C_1}\right) = \frac{\sqrt{\pi_{17}} C_2}{(\pi_{17} C_3 + z_{\max})^2},$$

where

$$C_1 = \frac{1}{2}\sqrt{k_p c_{01} \tau_{d1} \sigma_0'}, \quad C_2 = \frac{16 c_{01} \sigma_0'^2 C_1}{3\pi_1^2 \alpha^2 \tau_{d1}^2 \big[u - u_a(1)\big]^2},$$
$$C_3 = \frac{2\tau_{d1}\sigma_0'}{3k_p\alpha},$$

with solution

$$\begin{aligned} z_{\max} = 2\sqrt{\pi_{17}} C_1 W\left[\frac{\exp\left(\dfrac{\sqrt{\pi_{17}} C_3}{2C_1} + \dfrac{1}{2\sqrt{\pi_{17}} C_1}\right)\sqrt{C_2}}{2\sqrt[4]{\pi_{17}} C_1}\right] \\ - \pi_{17} C_3, \end{aligned} \tag{A12}$$

where W is a Lambert function (Olver et al. 2010). The asymptotic analysis of (A12) for $\pi_{17} \ll 1$ yields

$$z_{\max} = 1 + O\big(\sqrt{\pi_{17}} \ln \pi_{17}\big) < 1. \tag{A13}$$

It is easy to show that

$$\frac{d^2}{dz^2}\tau_d(z_{\max}) = O\big(\sqrt{\pi_{17}}\big) < 0. \tag{A14}$$

Thus, $z_{\max}$ is indeed the maximum point.

d. Asymptotic equations for spray horizontal velocity

The asymptotic decomposition of (57)–(59) in powers of parameter π_{17} yields the following equations and interface conditions at zeroth and 1/2th order of the parameter

$$O(1): k_p^2 \tau_{d1} \sigma_0' c_{01} \frac{d^2 u_{w0}^i}{d\xi^2} - k_p u_{w0}^i = \ln z_0, \tag{A15}$$

$$\left.\frac{du_{w0}^i}{d\xi}\right|_{\xi=0^-}^{\xi=0^+} = 0; \tag{A16}$$

$$O\big(\sqrt{\pi_{17}}\big): k_p^2 \tau_{d1} \sigma_0' c_{01} \frac{d^2 u_{w1}^i}{d\xi^2} - k_p u_{w1}^i + \xi = 0, \tag{A17}$$

$$\frac{\pi_1 \tau_{d1}}{k_p \sigma_0' c_{01}}\big[u - u_{w0}^i(0)\big] + \frac{du_{w1}^i}{d\xi}(0^+) - \frac{du_{w1}^i}{d\xi}(0^-) = 0. \tag{A18}$$

Note that Eqs. (A15) and (A17) are valid for both negative and positive values of variable ξ in the region just above and below the wave-crest level.

REFERENCES

Andreas, E. L, 1998: A new sea spray generation function for wind speeds up to 32 m s^{-1}. *J. Phys. Oceanogr.*, **28**, 2175–2184, https://doi.org/10.1175/1520-0485(1998)028<2175:ANSSGF>2.0.CO;2.

——, 2004: Spray stress revisited. *J. Phys. Oceanogr.*, **34**, 1429–1440, https://doi.org/10.1175/1520-0485(2004)034<1429:SSR>2.0.CO;2.

Barenblatt, G. I., 1953: On the motion of suspended droplets in a turbulent flow. *Prikl. Mat. Mekh.*, **7** (3), 261–274.

——, and G. S. Golitsyn, 1974: Local structure of mature dust storms. *J. Atmos. Sci.*, **31**, 1917–1933, https://doi.org/10.1175/1520-0469(1974)031<1917:LSOMDS>2.0.CO;2.

——, A. J. Chorin, and V. M. Prostokishin, 2005: A note concerning the Lighthill "sandwich model" of tropical cyclones. *Proc. Natl. Acad. Sci. USA*, **102**, 11 148–11 150, https://doi.org/10.1073/pnas.0505209102.

Bianco, L., J.-W. Bao, C. W. Fairall, and S. A. Michelson, 2011: Impact of sea-spray on the atmospheric surface layer. *Bound.-Layer Meteor.*, **140**, 361–381, https://doi.org/10.1007/s10546-011-9617-1.

Black, P. G., and Coauthors, 2007: Air–sea exchange in hurricanes. Synthesis of observations from the coupled boundary layer air–sea transfer experiment. *Bull. Amer. Meteor. Soc.*, **88**, 357–374, https://doi.org/10.1175/BAMS-88-3-357.

Boussinesq, J., 1897: *Théorie de l'écoulement tourbillonnant et tumultueux des liquides dans les lits rectilignes á grande section.* Gauthier-Villars et Fils, 84 pp.

Clift, R., J. R. Grace, M. E. Weber, and M. F. Weber, 1978: *Bubbles, Drops, and Particles.* Academic Press, 380 pp.

Csanady, G. T., 1963: Turbulent diffusion of heavy particles in the atmosphere. *J. Atmos. Sci.*, **20**, 201–208, https://doi.org/10.1175/1520-0469(1963)020<0201:TDOHPI>2.0.CO;2.

Danon, H., M. Wolfshtein, and G. Hetsroni, 1977: Numerical calculations of two-phase turbulent round jet. *Int. J. Multiphase Flow*, **3**, 223–234, https://doi.org/10.1016/0301-9322(77)90002-7.

Donelan, M. A., B. K. Haus, N. Reul, W. J. Plant, M. Stiassnie, H. C. Graber, O. B. Brown, and E. S. Saltzman, 2004: On the limiting aerodynamic roughness of the ocean in very strong winds. *Geophys. Res. Lett.*, **31**, L18306, https://doi.org/10.1029/2004GL019460.

Dritselis, C., and N. S. Vlachos, 2008: Numerical study of educed coherent structures in the near-wall region of a particle-laden channel flow. *Phys. Fluids*, **20**, 055103, https://doi.org/10.1063/1.2919108.

——, and ——, 2011: Numerical investigation of momentum exchange between particles and coherent structures in low re turbulent channel flow. *Phys. Fluids*, **23**, 025103, https://doi.org/10.1063/1.3553292.

Druzhinin, O. A., 1995a: Dynamics of concentration and vorticity modification in a cellular flow laden with solid heavy particles. *Phys. Fluids*, **7**, 2132–2142, https://doi.org/10.1063/1.868756.

——, 1995b: On the two-way interaction in two-dimensional particle-laden flows: The accumulation of particles and flow modification. *J. Fluid Mech.*, **297**, 49–76, https://doi.org/10.1017/S0022112095003004.

Eaton, J. K., and J. R. Fessler, 1994: Preferential concentration of particles by turbulence. *Int. J. Multiphase Flow*, **20**, 169–209, https://doi.org/10.1016/0301-9322(94)90072-8.

Elghobashi, S. E., and T. Abou-Arab, 1983: A two-equation turbulence model for two-phase flows. *Phys. Fluids.*, **26**, 931–938, https://doi.org/10.1063/1.864243.

Fairall, C. W., J. D. Kepert, and G. J. Holland, 1994: The effect of sea spray on surface energy transports over the ocean. *Global Atmos. Ocean Syst.*, **2**, 121–142.

——, M. L. Banner, W. L. Peirson, W. Asher, and R. P. Morison, 2009: Investigation of the physical scaling of sea spray spume droplet production. *J. Geophys. Res.*, **114**, C10001, https://doi.org/10.1029/2008JC004918.

Gore, R. A., and C. T. Crowe, 1989: Effect of particle size on modulating turbulent intensity. *Int. J. Multiphase Flow*, **15**, 279–285, https://doi.org/10.1016/0301-9322(89)90076-1.

Haus, B. K., D. Jeong, M. A. Donelan, J. A. Zhang, and I. Savelyev, 2010: Relative rates of sea–air heat transfer and frictional drag in very high winds. *Geophys. Res. Lett.*, **37**, L07802, https://doi.org/10.1029/2009GL042206.

He, H., Q. Wu, D. Chen, J. Sun, C. Liang, W. Lin, and Y. Xu, 2018: Effects of surface waves and sea spray on air-sea fluxes during the passage of Typhoon Hagupit. *Acta Oceanol. Sin.*, **37**, 1–7, https://doi.org/10.1007/s13131-018-1208-2.

Hetsroni, G., and M. Sokolov, 1971: Distribution of mass, velocity, and intensity of turbulence in a two-phase turbulent jet. *J. Appl. Mech.*, **38**, 315–327, https://doi.org/10.1115/1.3408779.

Hinze, J. O., 1975: *Turbulence.* McGraw-Hill, 790 pp.

Jakobsen, H. A., 2008: *Chemical Reactor Modeling: Multiphase Reactive Flows.* Springer, 1244 pp.

Kudryavtsev, V. N., 2006: On the effect of sea drops on the atmospheric boundary layer. *J. Geophys. Res.*, **111**, C07020, https://doi.org/10.1029/2005JC002970.

Levy, Y., and F. C. Lockwood, 1981: Velocity measurements in a particle laden turbulent free jet. *Combust. Flame*, **40**, 333–339, https://doi.org/10.1016/0010-2180(81)90134-6.

Lighthill, J., 1999: Ocean spray and the thermodynamics of tropical cyclones. *J. Eng. Math.*, **35**, 11–42, https://doi.org/10.1023/A:1004383430896.

Ling, S. C., and T. W. Kao, 1976: Parameterization of the moisture and heat transfer process over the ocean under whitecap sea states. *J. Phys. Oceanogr.*, **6**, 306–315, https://doi.org/10.1175/1520-0485(1976)006<0306:POTMAH>2.0.CO;2.

Ma, H., A. V. Babanin, and F. Qiao, 2020: Field observations of sea spray under Tropical Cyclone Olwyn. *Ocean Dyn.*, **70**, 1439–1448, https://doi.org/10.1007/s10236-020-01408-x.

Makin, V. K., 2004: A note on the drag of the sea surface at hurricane winds. *Bound.-Layer Meteor.*, **115**, 169–176, https://doi.org/10.1007/s10546-004-3647-x.

Mestayer, P., and C. Lefauconnier, 1988: Spray droplet generation, transport, and evaporation in a wind wave tunnel during the humidity exchange over the sea experiments in the simulation tunnel. *J. Geophys. Res.*, **93**, 572–586, https://doi.org/10.1029/JC093iC01p00572.

Nayfeh, A. H., 2008: *Perturbation Methods.* Wiley, 437 pp.

Olver, F. W. J., D. W. Lozier, R. F. Boisvert, and C. W. Clark, 2010: *NIST Handbook of Mathematical Function.* Cambridge University Press, 968 pp.

Peng, T., and D. Richter, 2020: Influences of poly-disperse sea spray size distributions on model predictions of air-sea heat fluxes. *J. Geophys. Res. Atmos.*, **125**, e2019JD032326, https://doi.org/10.1029/2019JD032326.

Powell, M. D., P. J. Vickery, and T. A. Reinhold, 2003: Reduced drag coefficient for high wind speeds in tropical cyclones. *Nature*, **422**, 279–283, https://doi.org/10.1038/nature01481.

Rastigejev, Y., and S. A. Suslov, 2014: E–ε model of spray-laden near-sea atmospheric layer in high wind conditions. *J. Phys. Oceanogr.*, **44**, 742–763, https://doi.org/10.1175/JPO-D-12-0195.1.

——, and ——, 2016: Two-temperature non-equilibrium model of a marine boundary layer laden with evaporating ocean spray under high-wind conditions. *J. Phys. Oceanogr.*, **46**, 3083–3102, https://doi.org/10.1175/JPO-D-16-0039.1.

——, and ——, 2019: Effect of evaporating sea spray on heat fluxes in a marine atmospheric boundary layer. *J. Phys. Oceanogr.*, **49**, 1927–1948, https://doi.org/10.1175/JPO-D-18-0240.1.

——, ——, and Y.-L. Lin, 2011: Effect of ocean spray on vertical momentum transport under high-wind conditions. *Bound.-Layer Meteor.*, **141**, 1–20, https://doi.org/10.1007/s10546-011-9625-1.

Richter, D., and P. Sullivan, 2013: Momentum transfer in a turbulent, particle-laden Couette flow. *Phys. Fluids*, **25**, 053304, https://doi.org/10.1063/1.4804391.

——, and ——, 2014: Modification of near-wall coherent structures by inertial particles. *Phys. Fluids*, **26**, 103304, https://doi.org/10.1063/1.4900583.

Simonin, O., 1991: Prediction of the dispersed phase turbulence in particle-laden jets. *Proceedings of the Fourth International Symposium on Gas-Solid Flows*, ASME FED, Vol. **121**, American Society of Mechanical Engineers, 197–206.

——, and P. L. Viollet, 1990: Prediction of an oxygen droplets pulverization in a compressible subsonic coflowing hydrogen flow. *Numerical Methods for Multiphase Flows*. ASME FED, Vol. **91**, American Society of Mechanical Engineers, 73–82.

Sun, D., J. Song, X. Li, K. Ren, and H. Leng, 2021: A novel sea surface roughness parameterization based on wave state and sea foam. *J. Mar. Sci. Eng.*, **9**, 246, https://doi.org/10.3390/jmse9030246.

Tang, S., Z. Yang, C. Liu, Y. H. Dong, and L. Shen, 2017: Numerical study on the generation and transport of spume droplets in wind over breaking waves. *Atmosphere*, **8**, 248, https://doi.org/10.3390/atmos8120248.

Toffoli, A., A. V. Babanin, M. A. Donelan, B. K. Haus, and D. Jeong, 2011: Estimating sea spray concentration with the laser altimeter. *J. Atmos. Oceanic Technol.*, **28**, 1177–1183, https://doi.org/10.1175/2011JTECHO827.1.

Vanderplow, B., A. V. Soloviev, C. W. Dean, B. K. Haus, R. Lukas, M. Sami, and I. Ginis, 2020: Potential effect of bio-surfactants on sea spray generation in tropical cyclone conditions. *Sci. Rep.*, **10**, 19057, https://doi.org/10.1038/s41598-020-76226-8.

Van Dyke, M., 1964: *Perturbation Methods in Fluid Mechanics*. Applied Mathematics and Mechanics, Vol. **8**, Academic Press, 229 pp.

Veron, F., 2015: Ocean spray. *Annu. Rev. Fluid Mech.*, **47**, 507–538, https://doi.org/10.1146/annurev-fluid-010814-014651.

Wamser, C., and V. N. Lykossov, 1995: On the friction velocity during blowing snow. *Contrib. Atmos. Phys.*, **68**, 85–94.

Wilcox, D. C., 2006: *Turbulence Modeling for CFD*. 3rd ed. DCW Industries, 522 pp.

Wu, L., A. Rutgersson, E. Sahlee, and X. G. Larsen, 2015: The impact of waves and sea spray on modelling storm track and development. *Tellus*, **67A**, 27 967, https://doi.org/10.3402/tellusa.v67.27967.

Yudine, M. I., 1959: Physical considerations on heavy-particle diffusion. *Advances in Geophysics*, Vol. **6**, Academic Press, 185–191, https://doi.org/10.1016/S0065-2687(08)60106-5.

Zhao, D., and M. Li, 2019: Dependence of wind stress across an air–sea interface on wave states. *J. Oceanogr.*, **75**, 207–223, https://doi.org/10.1007/s10872-018-0494-9.